Glycosylphosphatidylinositol-anchoring is required for the proper transport and extensive glycosylation of a classical arabinogalactan protein precursor in tobacco BY-2 cells

Nagasato, Daiki
Graduate School of Bioresource and Bioenvironmental Science, Kyushu University

Sugita, Yuto
Graduate School of Bioresource and Bioenvironmental Science, Kyushu University

Tsuno, Yuhei
Graduate School of Bioresource and Bioenvironmental Science, Kyushu University

Tanaka, Rutsuko
Chikushigaoka High School

他

出版情報：Bioscience, Biotechnology, and Biochemistry. 87 (9), pp.991-1008, 2023-06-22. Oxford University Press
バージョン：

Glycosylphosphatidylinositol-anchoring is required for the proper transport and extensive glycosylation of a classical arabinogalactan protein precursor in tobacco BY-2 cells.

Daiki Nagasato[1], Yuto Sugita[1], Yuhei Tsuno[1], Rutsuko Tanaka[2], Maki Fukuda[3], Ken Matsuoka[1,3,4,*]

[1]Graduate School of Bioresource and Bioenvironmental Science, Kyushu University, Fukuoka, Japan

[2]Chikushigaoka High School, Fukuoka, Japan

[3]School of Agriculture, Kyushu University, Fukuoka, Japan

[4]Faculty of Agriculture, Kyushu University, Fukuoka, Japan

* Correspondence: Ken Matsuoka, Department of Bioscience and Biotechnology, Faculty of Agriculture, Kyushu University, 744 Motooka, Nishi-ku, Fukuoka 819-0395, Japan.

Email: kenmat@agr.kyushu-u.ac.jp

Running Head: Role of GPI-anchor on AGP transport and maturation

ABSTRACT

Many precursors of plant arabinogalactan proteins (AGPs) contains a C-terminal glycosylphosphatidylinositol **(**GPI)-anchoring signal. Using NtAGP1, a classical tobacco AGP, as a model, and green fluorescent protein (GFP) and sweet potato sporamin (SPO) as tags, we analyzed the localization and modification of AGP and its mutant without GPI-anchoring signal (AGPΔC) in tobacco BY-2 cells. The NtAGP1 fusion proteins migrated as large smear on SDS-polyacrylamide gel and these proteins also localized preferentially to the plasma membrane. In contrast, fusions of AGPΔC with GFP- and SPO yielded several forms: The largest were secreted, whereas others were recovered in the endomembrane organelles including vacuoles. Comparison of the glycan structures of the microsomal SPO-AGP and the secreted SPO-AGPΔC using antibodies against the glycan epitopes of AGP indicated that the glycan structures of these proteins are different. These observations indicate that GPI-anchoring is required for the proper transport and glycosylation of the AGP precursor.

Keywords: glycan epitope, vacuolar targeting, late secretory pathway, Golgi apparatus

Introduction

Arabinogalactan proteins (AGPs) are plant cell wall proteoglycans with diverse functions (Pereira *et al.* 2015; Hromadová *et al*. 2021). Most of them contain many arabinogalactan (AG)-type glycan chains attached to Hyp residues that are post-translationally generated by the action of prolyl hydroxylases (Showalter *et al*. 2010). These proteins are classified into at least five groups based on their domain composition (Showalter *et al*. 2010). One of these groups consists of precursors to the classical AGPs; each of these precursors is made up of a signal peptide for the translocation of the endoplasmic reticulum (ER) membrane, glycosylation domains with many proline residues, and a signal sequence for the attachment of a glycosylphosphatidylinositol (GPI) anchor (Showalter *et al*. 2010; Yeats *et al*. 2018). Some members of other classes of AGP precursor do not contain a GPI-anchoring signal (Showalter *et al*. 2010).

GPI anchors are a class of lipid anchors that retain proteins at the surface of the plasma membrane (PM), especially within the sphingolipid-sterol-rich lipid domain (Liu and Fujita 2020) by inserting the acyl chains of lipid at the outer leaflet of the PM. Based on analyses of mammalian cells and baker's yeast, the biosynthesis of GPI anchors and their subsequent modification during transport to the PM proceed as follows. First, the biosynthesis of the GPI anchor starts at the ER, and then the pre-assembled GPI anchor is transferred from the ER to the carboxy-terminus of proteins that contain the GPI-anchoring signal to yield a GPI-anchored protein. With the assistance of p24 proteins, GPI-anchored proteins are efficiently sorted into coat protein complex II (COPII) vesicles at the ER exit site and transported to the Golgi apparatus (Bernat-Silvestre *et al*. 2020; Muñiz and Riezman 2016). During the subsequent transport to the PM by passing through the Golgi apparatus, the lipid part of the anchor undergoes remodeling and changes its structure (Liu and Fujita, 2020).

Most of the orthologs of genes that are indispensable for the biosynthesis and remodeling of GPI anchors in mammals and yeast are found in higher plants (Beihammer *et al*. 2020). Only a limited number of genes that are predicted to be involved in this step have been characterized to date (Bernat-Silvestre *et al*. 2021; Lin *et al.* 2022; Xu *et al*. 2022), in part because some of their null mutants are embryo-lethal (Yeats *et al*. 2018).

The modification of AGP polypeptide starts at the ER and *cis*-side of the Golgi apparatus, where Pro residues are converted to Hyp residues by the action of prolyl-hydroxylases localized in the ER and the *cis*-side of the Golgi apparatus (Yuasa *et al*. 2005; Velasquez *et al*. 2015; Parsons *et al*. 2018). The subsequent addition of galactose to the Hyp residue by Hyp galactosyltransferases (Oka *et al*. 2010; Basu *et al*. 2013, 2015; Ogawa-Ohnishi and Matsubayashi 2015) and the building of the AG glycan on the galactose residue in the Golgi apparatus allows the maturation of the AGP precursor (reviewed in Showalter and Basu 2106). During or after maturation, glycosylated and GPI-anchored AGPs are transported to the PM, and some of them are released to the extracellular space by the action of phospholipase in the cell wall. Several enzymes involved in AGP glycan synthesis have been characterized (reviewed in Showalter and Basu 2016), still we need to characterize enzymes for the AGP glycan biosynthesis based on the complex structure of the AGP glycans from tobacco BY-2 cells and Arabidopsis (Tan *et al*. 2004; Tryfona *et al*. 2015; Showalter and Basu, 2016).

As both the remodeling of the GPI anchors and the maturation of AGP glycans takes place in the Golgi apparatus, there may be a linkage between these two modifications. The Golgi apparatus is an organelle located in the endomembrane transport system, and this system directs proteins to several destinations including the PM, extracellular space, and vacuoles. As such, GPI anchoring might play a role in the proper transport of proteins. However, this possibility has not been adequately investigated, especially with respect to the transport of AGP. It has been reported that GPI anchoring is indispensable for PM localization of the Citrin-fused FLA4 protein, a fasciclin-domain containing AGP in *Arabidopsis* (Xue *et al*. 2017). In this case, most of the green fluorescence of the mutant Citrin-FLA4 lacking a GPI-anchoring signal appeared to be retained in the ER, and only a part of the green fluorescence from this protein seemed to be secreted to the extracellular space, although this partial secretion was sufficient to complement the mutant phenotype of fla4 (Xue *et al*. 2017). Although this observation indicates that GPI anchoring is required for the proper localization of this protein, this observation may not be applicable to other classes of AGP; e.g., classical AGP, which does

not contain a fasciclin domain, and almost all of the mature polypeptide region is predicted to be heavily glycosylated with AG glycans (Showalter *et al*. 2010).

Here we investigated the role of GPI anchoring in the transport and glycosylation of tobacco NtAGP1 (GenBank no. BAU61512), which is a classical AGP expressed in tobacco BY-2 cells, by expressing two different protein-tagged versions in tobacco BY-2 cells. We present evidence that GPI anchoring is required for both the proper transport and the proper glycosylation of this protein.

Materials and Methods

An outline of the methods and critical information about the materials used in this study are provided next; more detailed information about the plasmid construction, cell fixation, cell fractionation, antibodies and immunological methods, microscopy, two-phase separation, and other assays are described in the Supplemental Materials and Methods.

Construction of plasmids

A tobacco cDNA clone, BY28237 (GenBank accession no. LC128049.1) encoding the NtAGP1 protein (GenBank accession no. BAU61512) was used for the construction of plasmids used herein. The fusion protein of green fluorescence protein (GFP) and NtAGP1, designated as GFP-AGP, was designed using this clone and a mutant GFP, i.e., sGFP(S65T) (Chiu *et al*. 1996). For the construction of sporamin (SPO) fusions, the coding sequence for the signal peptide and the mature SPO fusion construct (Δpro SPO; Matsuoka and Nakamura 1991) was used for the signal peptide-SPO region. All of the expression constructs were subcloned under the enhancer-duplicated CaMV 35S promoter in a plant expression vector pMAT137 (Yuasa *et al*. 2005) and used for transformation. The detailed methods used for the construction of plasmids are described in the Supplemental Materials and Methods.

Culture, transformation, fixation, and immunostaining of tobacco BY-2 cells

The cultures of tobacco BY-2 cells and its transformant expressing SPO-AGP were maintained as described (Tasaki *et al*. 2014). For immunostaining, BY-2 cells or its transformants were fixed and permeabilized and incubated with primary and secondary antibodies essentially as described (Yuasa *et al*. 2005). Seven-day-old cells (stationary phase) were used in all of the experiments except when stated otherwise in the figure legends.

Confocal microscopy and image analysis

The localizations of GFP-AGP and GFP-AGPΔC expressed in transformed BY-2 cells were visualized using a confocal laser scanning microscope (TCS SP8, Leica, Wetzlar, Germany) essentially as described (Tasaki *et al*. 2014). In some cases, Z-stack images were collected and converted to a rotating movie. To visualize the plasma membrane using FM 4-64 or cytoplasm using chloromethyl SNARF-1, cells were stained with either FM4-64 or chloromethyl SNARF-1 acetate as described (Yuasa *et al*. 2005). Confocal images of the red fluorescence of stained cells were collected as described above with adjustment of the excitation and emission wavelengths.

Antibodies

Rabbit anti-mitochondrial porin antiserum was generated as described in the Supplemental Materials and Methods. Antisera against SDS-denatured SPO (Matsuoka and Nakamura., 1991), affinity purified anti-native SPO (Matsuoka *et al*. 1995), affinity purified anti-plant Sec61 (Yuasa *et al*. 2005), anti-V-PPase (Toyooka *et al*. 2009), anti-PIP (Suga *et al*. 2001), and anti-GLMT1 (Liu *et al*. 2015) antibodies were used at the appropriate dilutions. The monoclonal anti-AGP glycan antibodies LM2 and LM6 (Yates *et al*. 1996), were purchased from PlantProbes (Leeds, UK). For the visualization of the antigen-antibody complex by immunoblotting or indirect immunostaining, Alexa Fluor 488 goat anti-rabbit IgG (H+L), Alexa Fluor 568 goat anti-rabbit IgG (H+L), Alexa Fluor 568 goat anti-mouse IgG (H+L), Alexa Fluor 568 goat anti-rat IgG

(H+L), Alexa Fluor 647 goat anti-rat IgG (H+L), and Alexa Fluor 647 goat anti-rat IgM (μ chain) were purchased from Invitrogen (Eugene, OR, USA).

SDS-PAGE and detection of fusion proteins

For the estimation of the size and extent of modification of the fluorescent fusion proteins, the proteins were separated by SDS-PAGE, and their fluorescence was recorded by direct scanning of the gel using an image analyzer (Typhoon 9600, GE Healthcare Bio-Science, Chicago, IL) as described (Tasaki *et al*. 2014). For the detection of SPO fusion proteins and AGP glycan, immunoblotting was carried out as described (Oda *et al*. 2020) using appropriate primary and fluorescence-tagged secondary antibodies.

For the comparison of the reactivities of SPO-AGP and secreted SPO-AGPΔC against anti-glycan antibodies, we performed an adjustment of the loading of SPO-AGP in the microsomes and secreted large form of SPO-AGPΔC after semi-quantitative immunoblotting using anti-SPO antibody. Thereafter the volumes of the microsomes and the medium that gave nearly identical intensity were used for comparison by immunoblotting using anti-glycan antibodies.

Immunoprecipitation

Immobilized anti-native SPO was prepared as described (Matsuoka *et al*. 1995). Immunoprecipitation was performed essentially as described by Matsuoka and Nakamura (1991), except that the immobilized antibody was used instead of the anti-SPO serum and protein A Sepharose.

Subcellular fractionation of cells

Cells and media were separated from the suspension culture by filtration. For the differential centrifugation analyses, cells were mixed with buffer and disrupted using a Parr Cell Disruption Bomb (Parr Instruments, Moline, IL). The disrupted suspension was subjected to differential centrifugation. The precipitates after the 1,000*g*, 10,000*g*, and 100,000*g* centrifugations as well as the supernatant of the final spin

were designated as P1, P10, P100, and S fractions, respectively. In some case, P1 fraction was washed twice with Tris-buffered saline and used as cell wall fraction. For the fractionation of endomembrane organelles and the plasma membrane, microsomes prepared from cells were separated by linear sucrose density gradient centrifugation essentially as described by Matsuoka *et al*. (1997). Protoplasts were prepared as described by Nagata *et al.* (1981). Vacuoplasts and cytoplasts were prepared from protoplasts as described by Sonobe (1990).

Fractionation of GPI-anchored proteins by two-phase separation using Triton X-114

Pre-condensation of the nonionic detergent Triton X-114 and the fractionation of GPI-anchored proteins were performed as described by Murata *et al*. (2012) with minor modifications. In some cases,6.5 x 10^{-3} units of PI-PLC (phospholipase C, phosphatidylinositol-specific from *Bacillus cereus*) (Sigma-Aldrich, St. Louis, MO) were included during the incubation.

Cycloheximide treatment

Twenty mL of the 7-day old SPO-AGP culture was transferred to a 100-mL Erlenmeyer flask, and 200 μL of 1 mM cycloheximide and was added to the flask. The resulting flask was shaken in the dark at 26°C at 130 rpm. At 0, 3, and 24 hr of incubation, 1 mL of the culture was collected from the flask. Cells were collected by centrifugation, mixed with an equal amount of SDS-sample buffer, and lysed by sonication. After heating, equal volumes of protein-solubilized solution were subjected to SDS-PAGE and immunoblotting. As a control, water was used instead of cycloheximide solution.

Enzymes and protein assays

The α-mannosidase activity was measured as described (Boller and Kende, 1979) using *p*-nitrophenyl phosphate as a substrate. Protein concentrations were measured using a DC protein assay kit (Bio-Rad, Hercules, CA).

Results

Expression of the GFP-NtAGP1 fusion protein and its mutant without a GPI-anchoring signal in tobacco BY2-cells

The NtAGP1 was used as a model protein for classical AGP in this study. The amino acid sequence of this protein is nearly identical to that of *Nicotiana alata*-style AGP (Du *et al*. 1994). NtAGP1 is encoded by the expressed sequence tag (EST) clone BY28237 isolated from the mixture of cDNA prepared from various hormone-treated BY-2 cells (Galis *et al*. 2006). Four EST clones that have identical or nearly identical nucleotide sequences have been identified in our EST collections (Suppl. Table S1). Among them, three were obtained from the cDNA library from the hormone-treated BY-2 cells (Galis *et al*. 2006), and the fourth was from the mixture of cDNA prepared from lag-, log- and stationary growth-phase cells (Matsuoka *et al*. 2004). An expression analysis using microarrays (Matsuoka *et al*. 2004) indicated that the expression level of all of these clones was higher than average in both lag and log phases, with nearly equal levels of expression at the stationary phase (Suppl. Table S1). A BLASTN search against tobacco EST sequences using the nucleotide sequence for NtAGP1 identified 43 EST sequences (Suppl. Table S2). These sequences were obtained from a number of different cDNA libraries from various tobacco organs, including a female gamete, two-celled proembryo, leaf, flower, root, germinating seeds, and mixture of several tissues. NtAGP1 and its orthologous genes are thus expressed in many tobacco organs and at major growth phases of tobacco BY-2 cells.

The precursor to NtAGP1 consists of 132 amino acids (aa): a 21-aa signal peptide, an 86-aa glycosylation domain, and a C-terminal GPI-anchor signal, of which the last 25-aa are cleaved (Eisenhaber *et al*. 2003). Within the glycosylation region there are 23 Pro residues, most of which are surrounded with amino acids that make up the targeting sites for prolyl hydroxylases (Shimizu *et al*. 2005, Duruflé *et al*., 2017). Among these proline residues, 15 fit to the arabinogalactosylation site (Shimizu *et al.* 2005, Duruflé *et al*., 2017), and the other eight are contiguous prolines that might form the site for the attachment of oligo-arabinose (Xu *et al*. 2008). Because most of the distances between the proline residues in NtAGP1 are ≤5 aa,

and because the minimum length of a peptide epitope is six aa residues (Singh *et al*. 2013), we thought that it would be almost impossible to generate an antibody against the peptide sequence of NtAGP1 to detect the native protein in tobacco tissues and cells. We thus adopted the alternative approach of expressing fusion proteins consisting of NtAGP1 and protein tags and characterizing these proteins in tobacco BY-2 cells.

We first generated a construct for the expression of a fusion protein containing green fluorescence protein (GFP) between the signal peptide and the subsequent region of NtAGP1 (GFP-AGP). We also generated a mutant of this protein without a GPI-anchoring signal (GFP-AGPΔC) and a signal peptide with GFP only (GFP) (Fig. 1a). These proteins as well as the fusion proteins of the PM water channel and GFP (PIP-GFP: Yamauchi *et al*. 2003) were expressed in tobacco BY-2 cells, and the resulting transformed cells were cultured in suspension.

We then analyzed the GFP fluorescence of proteins in these transformed cell cultures that were grown for either 3 days (to the logarithmic growth phase) or 7 days (to the stationary growth phase) after the separation of proteins by sodium dodecyl sulfate-polyacrylamide gel electrophoresis (SDS-PAGE) and fluorescence recording (Fig. 1b). The fluorescence of GFP-AGP migrated as a large smear at around the 200-kDa position, and the intensity of this signal was stronger at 7 days. In the case of GFP-AGPΔC, at least three smear bands were observed: two bands that migrated to the 120-kDa and 48-kDa positions, and a relatively sharp band that migrated to around the 37-kDa position, the size of which corresponded to the non-glycosylated form of this approx. 35-kDa protein (Fig. 1b). The control proteins, GFP and PIP-GFP, migrated to the corresponding position on the SDS-polyacrylamide gel, as expected.

To determine the localization of these GFP fusion proteins, cultures of the transformed cells were separated into medium, cell wall, cellular membrane, and cellular soluble fractions. Proteins in these fractions were separated, and the distribution of the GFP fusion proteins was analyzed (Fig. 1c). GFP-AGP was recovered predominantly in the membrane fraction and to a lesser extent in the soluble fraction, and trace amounts were present in the cell walls and culture medium. In the case of GFP-AGPΔC, most of the large smear was recovered in the medium, and a small amount of this form was also found in the membrane and

soluble fractions. In contrast, almost all of the 48-kDa form was recovered in the membrane fraction, and the smallest 37-kDa form was recovered in the soluble fraction. In the case of PIP-GFP, which was used as the fractionation control, most of this protein was recovered in the membrane fraction with a trace amount in the cell walls, and faint signals of smaller forms, possibly truncated ones, were detected in the soluble fraction.

We next addressed the distribution of the GFP fluorescence from 7-day-old cells expressing either GFP-AGP or GFP-AGPΔC by a confocal laser scanning microscopy (CLSM) examination (Fig. 2). Almost all of the green fluorescence in the GFP-AGP-expressing cells was localized at the cell surface, possibly at the PM, and a weak signal was observed in the vacuoles as well as in unidentified punctate structures (Fig. 2, GFP-AGP). The intensities of fluorescence varied in the cells, and the cell-surface signal seemed nonuniform. In contrast to the cell-surface pattern of GF-AGP signal, cells expressing GFP-AGPΔC did not show such a pattern of fluorescence; they did exhibit weak green fluorescence in the vacuoles with an unidentified punctate structure with green fluorescence close to the cell wall (Fig. 2, GFP-AGPΔC).

To determine whether the GFP-AGP signal was localized in the PM, we incubated the cells for 5 min with FM 4-64 to visualize the plasma membrane, and both the GFP and FM 4-64 fluorescence were recorded (Fig. 3a). The GFP and FM 4-64 fluorescence colocalized well at the edges of the cells. The quantification of signal intensities on a line along the short axis at the middle of the cell (Fig. 3a, merged image, yellow line) indicated that the majority of the GFP fluorescence merged with the FM 4-64 fluorescence (Fig. 3a graph), although some GFP signal was also observed at the inside of the FM 4-64 signal.

To confirm whether a significant proportion of green fluorescence from GFP-AGP-expressing cells was localized to the PM, we stained the cells with FM 4-64 and observed the cells under plasmolysis (Fig. 3b). The clear lines of a green fluorescence signal, which corresponded to Hechtian strands, were visible between the PM and cell walls. At the same position, Hechtian strands with FM 4-64 fluorescence were present. Some of the fluorescence also seems attached to the cell wall, and some was present in the cell. These observations suggested that the majority of GFP-AGP was localized to the PM although some of it was present in intracellular structures.

To further confirm whether the majority of the GFP-AGP signal at the edge of the cells indicates the PM localization, we stained the cytoplasm with 5- (and 6-) chloromethyl SNARF-1 acetate (SNARF) and compared the localization of the GFP fluorescence with that of SNARF (Fig. 3c). The majority of the SNARF fluorescence localized close to the cell wall, in a pattern which was similar to that of GFP. However, a close inspection of the merged images and the quantification of signal intensities on a line along the short axis at the middle of the cell (Fig. 3b, merged image, yellow line) indicated that the peaks of the GFP fluorescence were located one or two pixels outside of the peak of SNARF fluorescence (Fig. 3b graph). These observations further confirmed that a significant proportion of GFP-AGP was localized to the PM.

As described above, optical section images suggested that the GFP fluorescence of GFP-AGP on the plasma membrane was not distributed evenly on the plasma membrane. To assess the non-uniform localization of GFP-AGP at the PM, we collected Z-stack images by CLSM and then reconstituted a 3D movie (Suppl. Movie S1). The nonuniform distribution of GFP fluorescence was apparent in the reconstituted 3D movie. These data indicated that GFP-AGP was predominantly localized to the PM, with a nonuniform distribution. Although these data suggested that the majority of the NtAGP1 is localized to the PM, we could not confirm this localization based on the result of the expression of only one fusion protein, and it was difficult to further characterize GFP-AGP, for several reasons. (1) The green fluorescence from GFP-AGP was unstable in the stably transformed tobacco BY-2 cells, and within six weeks of subculture, almost all of the cells stopped emitting green fluorescence. (2) The signal peptide-GFP fusion protein was not fully secreted to the culture medium from tobacco BY-2 cells (Mitsuhashi *et al*. 2000). Thus, GFP alone may not be a good cargo for secretion. (3) We have a fluorescence pulse-chase system that uses a photo-convertible fluorescence protein, monomeric Kikume Green-Red (mKikGR) (Habuchi *et al*. 2008) which has a higher-order structure that is similar to that of GFP, to monitor the turnover of proteins (Abiodun and Matsuoka 2013). We thus attempted to apply this system to address the transport of NtAGP1 by expressing the fusion protein of mKikGR and NtAGP1 in tobacco BY-2 cells. Unfortunately, the fusion protein migrated with three distinct bands: a weak large smear that migrated at a position similar to that of GFP-AGP, a predominant band around 60 kDa, and a

weaker band around 50 kDa (Suppl. Fig. S1). We therefore tested the transport and modification of NtAGP1 using a protein that is structurally distinct from GFP as a tag in order to determine the localization and transport of this protein and its mutant lacking a GPI-anchoring signal.

Expression and localization of the SPO-NtAGP1 fusion protein and its mutant lacking an GPI-anchoring signal in tobacco BY-2 cells

We used sweet potato SPO as another protein tag to address the transport, localization, and modification of NtAGP1 and its derivative lacking a GPI-anchoring signal. SPO is a monomeric soluble and non-glycosylated storage protein of sweet potato (Maeshima *et al.* 1985) localized in the vacuoles (Hattori *et al*. 1988). The expression of a mutant precursor to SPO, which does not contain the propeptide region but does contain the signal peptide for secretion, allowed the efficient secretion of this protein to the medium from transformed tobacco BY-2 cells (>90% of this pulse-labeled protein is secreted within 2 h of chase), and the kinetics of secretin is comparable with other major secretory proteins from tobacco BY-2 cells (Matsuoka and Nakamura 1991). The junction region between the propeptide and the mature SPO surrounding the 36th Pro residue consists of a cryptic Hyp *O*-glycosylation site for AG, and thus both a wild-type precursor to SPO as well as mutant precursors with a disrupted vacuolar targeting signal are *O*-glycosylated when expressed in tobacco BY-2 cells (Matsuoka *et al*. 1995, Matsuoka and Nakamura 1999).

The efficiency of the secretion of mutants with a disrupted vacuolar targeting signal is comparable to that of the mutant without the propeptide (Matsuoka and Nakamura 1999). In other words, the secretion efficiency of SPO is not affected by the presence or absence of *O*-glycosylation. We thus chose SPO as another protein tag to analyse the transport and modification of NtAGP1 and its mutant lacking a GPI-anchoring signal.

The expression constructs for the signal peptide-SPO-mature NtAGP1 with a GPI-anchoring signal (SPO-AGP) were expressed in tobacco BY-2 cells, as were the expression constructs for the signal peptide-SPO-mature NtAGP1 without a GPI-anchoring signal (SPO-AGPΔC) (Fig. 4a). Cell and medium fractions

were prepared from stationary-grown transformed BY-2 culture, and then the intra- and extra-cellular localizations of SPO or its fusion proteins in these fractions were examined by immunoblotting either directly without immunoprecipitation (Fig. 4b) or after target proteins were recovered by immunoprecipitation (Fig. 4c). Immunoblotting without immunoprecipitation gave cross-reacted protein bands in proteins from non-transformed cells (Fig. 4b, WT). Such signals were absent after immunoprecipitation (Fig. 4c, WT). However, our comparison of the intensities of SPO-related signals on many immunoblots obtained under both these conditions indicated that the recovery by immunoprecipitation varied among the proteins, especially SPO-AGP. We thus did not use immunoprecipitation for the subsequent quantitative analysis, and we always included a negative control from non-transformed cells.

SPO-AGP was detected as a smear band close to the top of the SDS-polyacrylamide gel (Fig. 4b, c). This observation indicated that SPO-AGP was glycosylated. Most of the smear-migrating protein was recovered in the cell fraction (Fig. 4b). In contrast, SPO-AGPΔC was detected as three distinct species with different migration positions; a large form that migrated at the 90–120-kDa position, an intermediate form at the 36-kDa position and a small one at the 22-kDa position (Fig. 4b, c). A specific band that migrated at the front of the electrophoresis gel may have been the degradation product of SPO (Fig. 4b). A large form of SPO-AGPΔC was detected in both the cell and medium fractions. Because the calculated molecular weight of non-glycosylated SPO-AGPΔC is 27.5, this observation indicated that most of the large-form SPO-AGPΔC was glycosylated and secreted into the extracellular space. The intermediate and small forms of SPO-AGPΔC were detected in cell fractions. This observation suggests that they were localized in the cells. The small form may be the degradation product, since its size (22 kDa) was similar to that of SPO (Fig. 4c) and smaller than the calculated size of the non-glycosylated form of SPO-AGPΔC.

To reveal the intracellular localization of SPO-AGP and SPO-AGPΔC, we performed subcellular fractionation by differential centrifugation. Cell lysates were centrifuged at 1,000*g* and the precipitate, defined as the P1 fraction (which contained unbroken cells, nuclei, cell walls and cell wall-attached PM) was collected. The supernatant was centrifuged at 10,000*g* and the precipitate (P10), which contained most of the

mitochondria and plastids, was collected. The resulting supernatant was further centrifuged at 100,000*g* and the obtained precipitate (P100) contained microsomal membranes. The supernatant, which was defined as the S fraction, was also collected. SPO-AGP was detected in the P1, P100, and S fractions (Fig. 4d). In the case of SPO-AGPΔC, the large and small forms were detected in the P1 and S fractions, while the intermediate form was observed in all fractions (Fig. 4e).

To address the localization of SPO-AGP, which was recovered in the P100 fraction, we prepared microsomal membranes from transformed BY-2 cells expressing SPO-AGP using buffers containing either $MgCl_2$ or EDTA, and we then separated the membranes by equilibrium sucrose density gradient centrifugation in the presence or absence of Mg^{2+}, respectively. The distribution of SPO-AGP in these separated fractions was examined by immunoblotting (Fig. 5a). The distributions of marker proteins were also analyzed by immunoblotting with specific antibodies: Sec61 for the ER (Yuasa *et al*. 2005), vacuolar pyrophosphatase (V-PPase) for tonoplast (Toyooka *et al*. 2009), GLMT1 for the Golgi apparatus (Liu *et al*. 2015), plasma membranous ATPase (P-ATPase) for the PM (Toyooka *et al*. 2009) and the PM water channel (PIP) for the PM (Suga *et al*. 2001). In the presence of Mg^{2+} (Fig. 5a, +$MgCl_2$), SPO-AGP migrated in several fractions, mainly in the fractions corresponding to 41–44(w/w)% sucrose. Quantification of the intensities of these immunoblot signals indicated that the migration pattern of SPO-AGP was similar to those of P-ATPase and PIP, the markers of the PM. In the absence of Mg^{2+} (Fig. 5a, +EDTA), SPO-AGP also migrated with a peak at around 41–43(w/w)% sucrose. This migration pattern was also similar to those of P-ATPase and PIP. These fractionation data indicated that SPO-AGP was localized to the PM.

To confirm the PM localization of SPO-AGP with a different method and to compare the localization of this protein with endogenous AGP, we fixed transformed cells expressing SPO-AGP with formaldehyde and stained them with anti-SPO or LM6 (Willats *et al*. 1998), which is a monoclonal antibody against oligo-arabinose epitope in both AGP glycan and rhamnogalacturonan I in pectin (Fig. 5b). LM6 recognized the glycan on SPO-AGP by immunoblotting (see below). For the control, non-transformed BY-2 cells were fixed and stained as well (Fig. 5b). During the fixation most of the cells shrank and separated from the cell walls,

and thus the localization at the cell wall and cells was easily distinguished, although some of the plasma membrane proteins were cross-linked to cell walls during fixation.

The staining of SPO-AGP-expressing cells with anti-native SPO antibody showed a clear signal at the cell wall, PM, and punctate structures in the cell, although a weak intracellular puncta signal was also observed when non-transformed cells were stained with this antibody (Fig. 5b). The pattern of staining of the SPO-AGP-expressing cells with anti-SPO antibody resembled the pattern of staining of wild-type cells with LM6 (Fig. 5b), although the SPO-AGP signal at the cell wall showed a more uneven distribution compared to that of LM6. Specificities of the staining including SPO-AGP dependency were confirmed by staining both SPO-AGP-expressing cells and wild-type cells with either and both antibodies (Suppl. Figs. S2, S3). The double immunostaining of SPO-AGP-expressing cells with anti-native SPO antibody and LM6 (Fig. 5c) revealed that both signals were colocalized well, although the SPO-AGP signal in the cells was more punctate compared to that of LM6. A comparison of signal intensities on a line along the short axis at the middle of the cell (Fig. 5c, merged image, yellow line) further confirmed that the majority of the SPO-AGP signal merged with the LM6 signal, especially at the cell wall and PM (Fig. 5c graph).

To address the stability of SPO-AGP, we measured the level of SPO-AGP after protein synthesis was stopped in the presence of cycloheximide. Although the average intensity of the SPO-AGP signal under the cycloheximide condition was lower than the control value, the difference was not significant (Suppl. Fig. S4). These observations suggest that SPO-AGP is not an unstable protein and that is localized mainly at the PM.

Intracellular localization of SPO-AGPΔC

We prepared protoplasts from transformed BY-2 cells expressing SPO-AGPΔC in order to determine which forms of SPO-AGPΔC were localized outside of the PM (Fig. 6a). The large form of SPO-AGPΔC was detected only in cells and was not detected in protoplasts. The intermediate-form protein was detected in both cells and protoplasts, although the amount was smaller in protoplasts than in cells. The small form of SPO-AGPΔC was detected in both fractions in nearly equal amounts. This result indicated that the large-form SPO-

AGPΔC was localized in the periplasm and cell wall; the intermediate SPO-AGPΔC was localized in both the periplasm and the cells, and the small SPO-AGPΔC was localized almost exclusively in the cells.

To address whether some of the intracellular SPO-AGPΔC was localized in vacuoles, we separated protoplasts into vacuoplast and cytoplast fractions and analyzed the amounts of the different forms of SPO-AGPΔC in these fractions. The vacuoplasts are composed of vacuoles surrounded by the PM, and cytoplasts are composed of cytoplasm, nuclei, and PM. We measured the protein concentration and assessed the α-mannosidase activity in the protoplast and cytoplast fractions. We then used SDS-PAGE to separate the proteins that were present in the protoplast and cytoplast fractions in nearly equal amounts and the proteins that were present in the protoplast and vacuoplast fractions in amounts that are almost equivalent to the levels of α-mannosidase activity. The different forms of SPO-AGPΔC in these fractions were detected by immunoblotting (Fig. 6b). Mitochondrial porin was used as a fractionation control. The intermediate SPO-AGPΔC was detected in the protoplast and cytoplast fractions in nearly equal amounts relative to the protein, whereas the small form was detected in both the protoplast and vacuoplast fractions in amounts similar to the activity of α-mannosidase. This result suggests that the small SPO-AGPΔC was localized in vacuoles and the intermediate SPO-AGPΔC was localized in other intracellular compartments.

To investigate the localization of the intermediate SPO-AGPΔC in cells, we prepared microsomal fractions from transformed BY-2 cells expressing SPO-AGPΔC in buffers containing either $MgCl_2$ or EDTA. The microsomal membranes were separated by equilibrium sucrose density gradient centrifugation in the presence or absence of Mg^{2+}, respectively. The distribution of the intermediate SPO-AGPΔC in these separated fractions was examined by immunoblotting and compared to the distributions of marker proteins in the secretory organelles (Fig. 6c). In the presence of Mg^{2+} (Fig. 6c, +$MgCl_2$), the intermediate SPO-AGPΔC migrated in several fractions with a peak at around 39–42(w/w)% sucrose. This migration pattern was similar to that of Sec61, a marker of the ER membrane. In the absence of Mg^{2+} (Fig. 6c, +EDTA), the intermediate SPO-AGPΔC also migrated with a peak at around 31–34(w/w)% sucrose, and the peak shifted to a lower-density position compared to that in the presence of Mg^{2+}. This shift corresponded to that of the migration

pattern of Sec61 (an ER marker). These fractions did not contain P-ATPase or PIP but did contain GLMT1, a marker of the Golgi apparatus. These fractionation data suggest that the intermediate form of SPO-AGPΔC is localized predominantly in the ER and partly in the Golgi apparatus.

NtAGP1 is a GPI-anchored protein

The NtAGP1 precursor contains a GPI-anchoring signal at its C-terminus. Our present analyses demonstrated that GFP-AGP and SPO-AGP are localized to the PM (Figs. 2, 5). To determine whether the GPI-anchoring signal on the NtAGP1 precursor is functional and whether the GPI anchor attached to NtAGP1 was responsible for attaching this protein to the PM, we analyzed the distribution of these fusion proteins recovered in the microsomal fraction by two-phase separation using the nonionic detergent Triton X-114. This nonionic detergent can be used to make a uniform solution at low temperature, which can then be separated into two phases, such as an aqueous (aqu) phase and a detergent-rich (det) phase, at higher temperature. By taking advantage of this characteristic of the nonionic detergent, a cell extract can be separated into soluble and peripheral membrane proteins that can be recovered in the aqu phase, plus integral membrane proteins as well as lipid-anchored proteins that can be recovered in the det phase (Bordier 1981).

Approximately half of the GFP-AGP (Fig. 7a, left) as well as almost all of the SPO-AGP (Fig. 7b, top left) and almost all of the PIP-GFP (an integral membrane protein used as an experimental control; Fig. 7a, right), was recovered in the det fraction. Under the same separation condition, almost all of the smear-migrating GFP-AGPΔC and SPO-AGPΔC were recovered in the aqu fraction. These observations suggested that about half of the GFP-AGP and almost all of the SPO-AGP were localized to the PM with their GPI anchors.

To address whether this membrane-association is actually mediated by the GPI anchor attached to these proteins, we carried out two-phase separation experiments in the presence of phosphatidylinositol-specific phospholipase C (PI-PLC), which can cleave the phosphodiester bond in a GPI anchor (reviewed by Hopper 2001). In the presence of PI-PLC, almost all of the GFP-AGP in the microsomal fraction was

recovered in the aqu phase (Fig. 7c, right). Likewise, about half of the SPO-AGP that was recovered in the TX-114 phase was recovered in the det phase (Fig. 7d, top). Under the same condition, vacuolar pyrophosphatase, which is an integral membrane protein used as a control, was recovered almost exclusively in the det phase (Fig. 7d, bottom). The difference in migration positions of SPO-AGP in the aqu and det phases after PI-PLC treatment may be due to the presence or absence of the GPI anchor. Indeed, such a difference in migration position before and after PI-PLC treatment was previously observed in mammalian ACA (Kojic and Terness, 2002). These observations indicated that (*i*) roughly half of both GFP-AGP and SPO-AGP was anchored to the PM by a GPI anchor that was sensitive to PI-PLC, and (*ii*) NtAGP1 is a GPI-anchored protein at the PM.

GPI anchoring seems required for the proper assembly of AGP glycan

We showed that the migration positions of the smear-migrating SPO-AGP and SPO-AGPΔC on SDS-polyacrylamide gel were different (Fig. 4a, B). We considered that this difference might be due to the difference in the AG glycan chains on these proteins. To address this possibility, we examined the reactivity of anti-AG glycan monoclonal antibodies (mABs) to these proteins. After titration of anti-SPO antibody reactivity against microsomal SPO-AGP and secreted SPO-AGPΔC by immunoblotting, approximately equal amounts of SPO fusion proteins were loaded on SDS-polyacrylamide gels. As controls, equal amounts of microsomal and media proteins from untransformed tobacco cells were loaded on the same gel, respectively. As expected, anti-SPO recognized both SPO-AGP and secreted SPO-AGPΔC with approximately the same intensity (Fig. 8a). Among the mABs that we tested, SPO-AGPΔC was specifically recognized by LM2 (Fig. 8b). Both proteins were recognized by LM6 (Fig. 8c). Other antibodies, namely PN16.4B4 (Norman *et al.* 1986), CCRC-M7 (Steffan *et al*. 1995), and MAC204 and MAC207 (Bradley *et al*. 1988), did not recognize either protein (data not shown). Because LM2 recognizes terminal β-glucuronic acid (β-GlcA) (Yates *et al*. 1996), the absence of the recognition of SPO-AGP by this antibody indicated that such a structure was absent in the glycan in SPO-AGP. This result also suggested that GPI anchoring is required for the extensive glycosylation of AGP.

Discussion

In this work we investigated the role of the GPI anchor in the transport and modification of NtAGP1, a classical AGP in tobacco BY-2 cells. The expression of the GFP fusion protein allowed us to detect the smear-migrating GFP fusion protein with low mobility on SDS-polyacrylamide gels (Fig. 1). This behavior of the fusion protein was consistent with the typical migration pattern of AGPs in many plant species (e.g., Putoczki *et al*. 2007; Lind *et al*. 1994; Maurer *et al*. 2010). In contrast, the fusion protein formed using another fluorescent protein, mKikGR (Habuchi *et al*. 2008), yielded one slow-migrating and two fast-migrating smear bands (Suppl. Fig. S1). To determine which of the observed migration behaviors of these fusion proteins represents the true nature of NtAGP1, we characterized another fusion protein with SPO and found that this fusion protein migrated as a slow-migration smear band on SDS-polyacrylamide gels (Fig. 4). We therefore concluded that the slow migration and formation of a smear band on SDS-polyacrylamide gels are characteristic of NtAGP1. These observations as well as the observation of multiple bands of GFP-fused *Arabidopsis* AGP4, which is a member of the classical AGP family that is transiently expressed in *Arabidopsis* seedlings (Bernat-Silvestre *et al*. 2020) also suggested that differences in the non-glycosylation domain of AGP may affect the degree of modification of classical AGPs.

Our analyses of the localization of GFP-AGP and SPO-AGP indicated that these proteins are predominantly localized to the PM (Figs. 2, 3, 5), and that both proteins are attached to the PM as GPI-anchored forms (Fig. 7). In addition, some of these proteins were present in intracellular structures (Figs. 3, 5) and in the medium. GFP-AGP fluorescence in the cell wall fraction was relatively weak, whereas the amount of SPO-AGP in the P1 fraction containing cell walls was relatively high (compare Fig. 1c, GFP-AGP, CW and Fig. 4d, P1). This discrepancy can be explained by the difference of sample preparation and the acid-sensitive nature of GFP. A significant proportion of SPO-AGP signal was observed in the cell walls (Fig. 5b), possibly due to the binding of PM to the cell walls. The cell wall fraction used in Fig. 1c was prepared by washing the P1 fraction thoroughly with buffer. Therefore, the amount of PM remaining in this fraction will be less than in the P1 fraction. As the periplasm and cell walls are acidic, this nature may destroy the chromophore of GFP to

decrease the fluorescence. These cell wall preparation method and nature of GFP can explain why the P1 fraction contained relatively higher SPO-AGP than the P100 fraction in Fig. 4d, while the cell wall fraction in Fig. 1c showed little GFP-AGP signal.

Collectively, these observations suggested that NtAGP1 is a GPI-anchored PM protein with a small pool in an uncharacterized intracellular structure, possibly related to an as-yet uncharacterized intermediate component of AGP synthesis (Poulsen *et al.* 2014). Some other population of NtAGP1 is also released to the extracellular space following the cleavage of its GPI anchor, possibly via the actions of phospholipase in the extracellular space. Similar low-level secretion of AGP or fluorescence protein-tagged AGP was reported in *Arabidopsis* (Darjania *et al*. 2002; Bernat-Silvestre *et al*. 2021; Xue *et al*. 2017). Such a low-level secretion of AGP might be the result of a slow release of this protein into the medium, since we observed that the cycloheximide treatment did not cause a significant decrease of cellular SPO-AGP within 24 hr (Suppl. Fig. S4). The presence of LM6 signal in both the cell wall and intracellular structures (Fig. 5) suggested that such a distribution is not specific to NtAGP1; rather it is common to other AGPs expressed in tobacco BY-2 cells, although we cannot rule out a possibility that significant proportion of the LM6 signals represent the presence of rhamnogalacturonan I.

The behavior to the two-phase separation assay as well as the sensitivity to PI-PLC were somewhat different between GFP-AGP and SPO-AGP (Fig 7). Microsomal GFP-AGP was recovered in both detergent and aqueous phases with similar extent and almost all the detergent-recovering GFP-AGP was sensitive to PI-PLC (Figs. 7a and c). In contrast, almost all the SPO-AGP was recovered in the detergent phase and around half of this protein was resistant to PI-PLC(Figs. 7b and d). These observations suggest that the GPI-anchor attached to SPO-AGP was more resistant to both endogenous phospholipase as well as the PI-PLC. It has been shown in mammalian cells that forms of GPI-anchored protein with acyl chain at the inositol ring in the anchor, those are intermediate forms of the GPI-anchor remodeling, are resistant to PI-PLC, although such form can also be exported from the ER (Liu et al., 2018). Based on the presence of gene conservation for GPI-anchor biosynthesis and maturation in eukaryotes (Yeats et al., 2017), such immature GPI-anchor on SPO-AGP

may be the reason of the resistance to PI-PLC. Similarly, partial resistance of fluorescent protein-tagged GPI-anchored proteins to PI-PLC in transgenic plants, and prevention of digestion by PI-PLC in mutants of the ER-localizing GPI-inositol deacylase genes have been reported (Bernat-Silvestre *et al*., 2021: Lin *et al*., 2022). In the mutants, fluorescent protein-tagged GPI-anchored proteins are partially targeted to the PM (Bernat-Silvestre *et al*., 2021: Lin *et al*., 2022).

If acyl removal from SPO-AGP is incomplete, how could such form be produced? SPO is an endogenous plant protein that is efficiently transported through the secretory pathway with similar kinetics to other major secretory proteins (Matsuoka and Nakamura, 1991). This secretory behavior can be explained by an idea that SPO is secreted through the default secretory pathway without having positive traffic information, but we cannot rule out the possibility that SPO has a positive signal that allows the rapid secretion. If this is the case, SPO-AGP would be exported from the ER without sufficient time for efficient remodeling of its GPI-anchor. Another possibility is that some of the endogenous plant GPI-anchored proteins have GPI-anchors with acyl chain in their final form. If this is the case, the nature of GFP, *i.e.* the non-plant protein loaded into plant secretory pathway, allowed to retain this fusion protein in the ER long enough to remove the acyl chain completely. Since only a limited numbers of the structure of GPI-anchor have been elucidated in plants, we cannot rule out these two possibilities. Future structural characterization of GPI-anchors in various proteins including AGPs will reveal which scenario will be feasible.

In contrast to the fusion proteins with an intact AGP with a GPI-anchoring signal, we detected mutant fusion proteins without a GPI-anchoring signal (i.e., GFP-AGPΔC and SPO-AGPΔC) as multiple bands at different migration positions on SDS-polyacrylamide gels (Figs. 1, 4). The glycosylated forms of these proteins that migrated the most slowly and the most readily formed smear bands were predominantly recovered in the medium fraction (Figs. 1, 4). The fractionation analysis of cells expressing these proteins indicated that the intermediate forms were recovered partly in the membranous organelles in the cells and partly in the periplasmic space (Figs. 1, 4). The migration positions of these proteins on SDS-polyacrylamide gels were slower than those of the calculated size of non-glycosylated forms of these proteins, suggesting that

these proteins are modified to some extent, probably with glycans. Purification of these proteins and analyses of their sugar compositions will clarify whether such modification takes place.

Our fractionation study of microsomes from SPO-AGPΔC-expressing cells indicated that the intermediate SPO-AGPΔC was localized in the ER with partial localization in the Golgi apparatus (Fig. 6). The smallest form of this protein, which was similar in size to SPO, was recovered in the soluble fraction from the cells, which consisted of the cytoplasm and vacuolar sap. The smallest form of SPO-AGPΔC was also recovered in the vacuoplast fraction. These observations indicated that some of the SPO-AGPΔC protein was transported to the vacuoles, while most of the AGP part of these proteins was cleaved off or degraded in the vacuoles. The weak green fluorescence in vacuoles of GFP-AGPΔC-expressing cells (Fig. 2), together with the rapid migration of GFP-AGPΔC, the putative degradation product of this protein, into the soluble fraction (Fig. 1c), may be the result of targeting of this protein to the vacuole. However, the method commonly used in autophagy studies to stabilize GFP fluorescence in the vacuole using the vacuolar ATPase inhibitor concanamycin A is not applicable to this study because this compound is a potent inhibitor of vacuolar targeting (Matsuoka *et al.*, 1997). Using a fluorescent protein that is more acid tolerant than GFP could be an alternative method to demonstrate that AGPΔC transport into the vacuole is independent of the protein tag, if such a protein does not affect glycosylation.

These observations indicated that GPI anchoring is not only essential for the proper and efficient transport of NtAGP1 to the plasma membrane or extracellular space but also required for the efficient glycosylation. Some of the inefficient-modified forms, i.e., the intermediate forms, were retained in the ER, and some of them could also be transported to the vacuoles for degradation. These observations are partly consistent with the case of a Citrin-tagged and GPI-anchoring signal-deleted fasciclin-like AGP mutant (Xue *et al.* 2017). In that case, most of the mutant protein was retained in the ER. In our present experiments, however, vacuolar localization was observed. This difference in vacuolar localization between the Xue *et al.* report and our present study might be attributable to either the different detection systems or different proteins used.

It has been reported that the vacuoles are scavenger organelles that degrade damaged proteins and organelles. In yeast, it has been shown that vacuolar targeting is a mechanism for degrading improperly folded proteins in the ER, and this transport is mediated by a receptor for vacuolar targeting (Hong *et al*. 1996). In plants, targeting of soluble proteins to the lytic vacuoles (such as the central vacuoles in tobacco BY-2 cells) is mediated by VSR proteins (reviewed in Shimada *et al*. 2018). Large and hydrophobic residues, such as Ile and Leu, in the vacuolar-sorting determinants in proteins play a pivotal role in the targeting (Ahmed *et al*. 2000; Brown *et al*. 2003; Matsuoka and Nakamura 1995, 1999; Paris *et al*. 1997). It is thus interesting that inefficient glycosylation of SPO-AGPΔC may cause the exposure of a large and hydrophobic side chain in the mature region of AGP, and this characteristic of SPO-AGPΔC may have allowed the targeting of this protein to the vacuole after recognition by VSR proteins, as in the case of yeast (Hong *et al*. 1986). In fact, the SPLA sequence at aa positions 67–70 of the NtAGP1 precursor, the Pro residue in which is predicted as partially converted to Hyp (Shimizu *et al*., 2005), resembles the NPIR vacuolar sorting determinants of SPO and aleurain propeptides (Matsuoka and Nakamura 1995, 1999; Paris *et al*. 1997). Therefore, this region may be a candidate for a region that undergo inefficient glycosylation and consequently interact with VSR.

Not only the mislocalization but also alteration of the glycan moiety was observed in the secreted SPO-AGPΔC from SPO-AGP (Fig. 8). Secreted SPO-AGPΔC was recognized by the mAB LM2, which was shown to recognize β-GlcA residues in AG glycan (Yates *et al*. 1996). It has been shown that the structure of the glycan moiety of artificial AGP secreted from tobacco BY-2 cells contains β-GlcA, which is further modified partly by rhamnose (Tan *et al*. 2004, 2010). In addition, the β-GlcA moiety of AGP is sometimes methylated by the action of DUF576-family methyltransferases (Temple *et al*. 2019). It is thus possible that (*i*) the glycan structure of secreted SPO-AGPΔC is similar to that of the artificial AGPs, which contain a terminal β-GlcA, whereas such a structure is absent in SPO-AGP, and (*ii*) this difference is achieved by an efficient modification with rhamnose or methyl residues. Further analyses of the sugar compositions of the purified SPO-AGP and secreted SPO-AGPΔC proteins are necessary to fully explore these possibilities.

What causes the difference in glycan structure between SPO-AGP and secreted SPO-AGPΔC? One possible answer may be related to the difference in transport routes of these proteins in the late secretory pathway, with different distributions of the enzymes responsible for modification for the AGP glycan. A study of tobacco protoplasts using a GFP-tagged pectin methylesterase inhibitor protein and its mutant without a GPI-anchoring signal revealed that the late transport pathways of these proteins are different (De Caroli *et al*. 2011). The DUF576-family methyltransferases that act against AGP glycan have been detected not only in the Golgi apparatus but also in small punctate structures that are distinct from the Golgi apparatus (Temple *et al*. 2019). Similarly, a subset of glycosyltransferases involved in AGP glycan biogenesis was identified in a non-Golgi and non-TGN (*trans*-Golgi network) punctate structure (Poulsen *et al*. 2015). An analysis of the secretome of *Arabidopsis* indicated that there are at least two distinct secretory pathways in *Arabidopsis* leaf cells (Uemura *et al*. 2019). One of these pathways, which depends on SYP4-type SNAREs, is involved in the secretion of many hydrolases (Uemura *et al*. 2019). In an analysis focusing on AGP in the data generated and described in that paper (PRIDE dataset identifier PXD009099 by H. Nakagami *et al*.), only a small fraction of AGPs with a GPI-anchoring signal (18%) showed significantly high abundance in apoplasts in a wild-type relative to a mutant with SYP4-type SNARE proteins (Suppl. Table S3).

In contrast, when the same approach was taken against two groups of secretory hydrolases, i.e., pectic-lyase like proteins without a GPI-anchoring signal and β-galactosidase, a greater proportion of these proteins showed a high level of secretion in the wild-type compared to the mutant SYP4-type SNARE proteins (35% and 38%, respectively). In *Arabidopsis*, the SYP4-type SNAREs are localized in not only the TGN adjusting the Golgi apparatus but also a small punctate structure that is called the Golgi-independent TGN or free TGN (Viotti *et al*. 2010; Kang *et al*. 2011; Uemura *et al*. 2014). A similar structure called a secretory vesicle cluster (SVC), which is involved in pectin secretion, is present in tobacco BY-2 cells (Toyooka *et al*. 2009). Analyses of the proteome and glycome of secretory vesicles marked with SYP61 indicated that these secretory vesicles are rich in the SYP4-type SNARE proteins as well as glycans that are recognized by mABs against pectin (Drakakaki *et al*. 2012; Wilkop *et al*. 2019). Although glycans in the same vesicle fraction are also recognized

by mABs against AGP, this recognition is weaker than that in the cell wall fraction, in contrast to the recognition by mABs that recognize pectin (Fig. 3 in Wilkop *et al.* 2019).

Collectively, these observations suggest that the GPI-anchored AGP precursor would be predominantly transported from the TGN to an uncharacterized punctate organelle, where a subset of glycosyltransferases and/or methyltransferases localize (Poulsen *et al*. 2015), and would then be transported to the PM after efficient modification of the glycan in the compartment (see graphical abstract, AGP). The absence of a GPI anchor in the AGP precursor prevents taking this route from the TGN, and it passes through the default secretion pathway; this mis-sorting limits the final maturation of AGP glycan (see graphical abstract, AGPΔC).

Another possible explanation for the difference in glycan structure is that the accessibility to the modification enzymes might not be efficient in the absence of a GPI anchor. Because most of the glycosyltransferases and methyltransferases in the secretory pathway are integral membrane proteins whose catalytic domains are located proximately to the phospholipid bilayer, the GPI anchoring of the AGP precursor will bring the protein close to the catalytic sites of these enzymes. Without a GPI anchor, such access would not be efficient, and this characteristic would prevent the efficient maturation of the glycan side chain. A third possibility is that the transport speed is different between SPO-AGP and SPO-AGPΔC, and this difference contributes to the difference in the glycan side chain. Future studies to address the pathways and kinetics of transport and modification of AGP using SPO-AGP as a model will reveal which scenario or combination of scenarios is most likely.

Acknowledgments

We thank Dr. Koji Yuasa of the RIKEN Plant Science Center for the production of recombinant mitochondrial porin and Mr. A. B. Nweke for improving the manuscript.

Supplemental material

Supplementary material is available at Bioscience, Biotechnology, and Biochemistry online.

Data Availability

NtAGP1 cDNA sequence data and its translated protein sequence are available in the GenBank with accession No. LC128049.

Author contribution

YT, RT, and KM performed the experiments on GFP fusion proteins. DN, YS, MF, and KM performed the experiments on SPO-fusion proteins. DN, YT, YS, and KM designed the experiments and analyzed the data. KM conceived the project and wrote the article with contributions from all the authors. All of authors critical read and approved the final manuscript.

Funding

This work was supported in part by a grant from the Japan Society for the Promotion of Science (JSPS) KAKENHI (no. 26292194 to K.M.).

Disclosure statement

No potential conflict of interest was reported by the authors.

References

Abiodun MO, Matsuoka K. Evidence that proliferation of Golgi apparatus depends on both de novo generation from the endoplasmic reticulum and formation from pre-existing stacks during the growth of tobacco BY-2 cells. *Plant Cell Physiol* 2013;54:541-54.

Basu D, Liang Y, Liu X et al. Functional identification of a hydroxyproline-o-galactosyltransferase specific for arabinogalactan protein biosynthesis in Arabidopsis. *J Biol Chem* 2013;288:10132-43.

Basu D, Wang W, Ma S et al. Two hydroxyproline galactosyltransferases, GALT5 and GALT2, function in arabinogalactan-protein glycosylation, growth and development in Arabidopsis. *PLoS One*. 2015;10:e0125624.

Becker Kojić ZA, Terness P. A novel human erythrocyte glycosylphosphatidylinositol (GPI)-anchored glycoprotein ACA. Isolation, purification, primary structure determination, and molecular parameters of its lipid structure. *J Biol Chem* 2002;277:40472-8.

Beihammer G, Maresch D, Altmann F et al. Glycosylphosphatidylinositol-anchor synthesis in plants: A glycobiology perspective. *Front Plant Sci* 2020;11:611188.

Bernat-Silvestre C, De Sousa Vieira V, Sanchez-Simarro J et al. p24 family proteins are involved in transport to the plasma membrane of GPI-anchored proteins in plants. *Plant Physiol* 2020;184:1333-47.

Bernat-Silvestre C, Sánchez-Simarro J, Ma Y et al. AtPGAP1 functions as a GPI inositol-deacylase required for efficient transport of GPI-anchored proteins. *Plant Physiol* 2021;187:2156-73.

Boller T, Kende H. Hydrolytic enzymes in the central vacuole of plant cells. *Plant Physiol* 1979;63:1123-32.

Bordier C. Phase separation of integral membrane proteins in Triton X-114 solution. *J Biol Chem* 1981;256:1604-7.

Bradley D, Wood E, Larkins A et al. Isolation of monoclonal-antibodies reacting with peribacteroid membranes and other components of pea root-nodules containing rhizobium-leguminosarum. *Planta* 1988;173:149-60.

Chiu W, Niwa Y, Zeng W et al. Engineered GFP as a vital reporter in plants. *Curr Biol* 1996;6:325-30.

Darjania L, Ichise N, Ichikawa S et al. Dynamic turnover of arabinogalactan proteins in cultured *Arabidopsis* cells. *Plant Physiol Biochem* 2002;40:69-79.

De Caroli M, Lenucci MS, Di Sansebastiano GP et al. Protein trafficking to the cell wall occurs through mechanisms distinguishable from default sorting in tobacco. *Plant J* 2011;65:295-308.

Drakakaki G, van de Ven W, Pan S et al. Isolation and proteomic analysis of the SYP61 compartment reveal its role in exocytic trafficking in *Arabidopsis. Cell Res* 2012;22(2):413-24.

Du H, Simpson RJ, Moritz RL et al. Isolation of the protein backbone of an arabinogalactan-protein from the styles of *Nicotiana alata* and characterization of a corresponding cDNA. *Plant Cell* 1994;6:1643-53.

Duruflé H, Hervé V, Balliau T et al. Proline hydroxylation in cell wall proteins: Is it yet possible to define rules? *Front Plant Sci* 2017;8:1802.

Eisenhaber B, Wildpaner M, Schultz CJ et al. Glycosylphosphatidylinositol lipid anchoring of plant proteins. Sensitive prediction from sequence- and genome-wide studies for Arabidopsis and rice. *Plant Physiol*. 2003;133:1691-701.

Habuchi S, Tsutsui H, Kochaniak AB et al. mKikGR, a monomeric photoswitchable fluorescent protein. *PLoS One*. 2008;3:e3944.

Hong E, Davidson AR, Kaiser CA. A pathway for targeting soluble misfolded proteins to the yeast vacuole. *J Cell Biol* 1996;135:623-33.

Hromadová D, Soukup A, Tylová E. Arabinogalactan proteins in plant roots - An update on possible functions. *Front Plant Sci* 2021;12:674010.

Kang BH, Nielsen E, Preuss ML et al. Electron tomography of RabA4b- and PI-4Kβ1-labeled *trans* Golgi network compartments in *Arabidopsis*. *Traffic* 2011;12:313-29.

Lin Z, Xie F, Triviño M et al. Self-incompatibility requires GPI anchor remodeling by the poppy PGAP1 ortholog HLD1. *Curr Biol* 2022;32:1909-23

Lind JL, Bacic A, Clarke AE et al. A style-specific hydroxyproline-rich glycoprotein with properties of both extensins and arabinogalactan proteins. *Plant J* 1994;6:491-502.

Liu J, Hayashi K, Matsuoka K. Membrane topology of Golgi-localized probable S-adenosylmethionine-dependent methyltransferase in tobacco (*Nicotiana tabacum*) BY-2 cells. *Biosci Biotechnol Biochem* 2015;79:2007-13

Liu Y, Guo X, Hirata T et al. N-Glycan-dependent protein folding and endoplasmic reticulum retention regulate GPI-anchor processing. *J Cell Biol* 2018;217:585-99.

Liu YS, Fujita M. Mammalian GPI-anchor modifications and the enzymes involved. *Biochem Soc Trans*. 2020;48:1129-38.

Matsuoka K, Higuchi T, Maeshima M et al. A vacuolar-type H^+-ATPase in a nonvacuolar organelle is required for the sorting of soluble vacuolar protein precursors in tobacco cells. *Plant Cell* 1997;9:533-46.

Matsuoka K, Nakamura K. Propeptide of a precursor to a plant vacuolar protein required for vacuolar targeting. *Proc Natl Acad Sci USA* 1991;88:834-8.

Matsuoka K, Nakamura K. Large alkyl side-chains of isoleucine and leucine in the NPIRL region constitute the core of the vacuolar sorting determinant of SPO precursor. *Plant Mol Biol* 1999;41:825-35.

Matsuoka K, Watanabe N, Nakamura K. O-glycosylation of a precursor to a sweet potato vacuolar protein, SPO, expressed in tobacco cells. Plant J. 1995;8:877-89.

Maurer JB, Bacic A, Pereira-Netto AB et al. Arabinogalactan-proteins from cell suspension cultures of *Araucaria angustifolia*. *Phytochemistry* 2010;71:1400-9.

Murata D, Nomura KH, Dejima K et al. GPI-anchor synthesis is indispensable for the germline development of the nematode *Caenorhabditis elegans*. *Mol Biol Cell* 2012;23:982-95.

Muñiz M, Riezman H. Trafficking of glycosylphosphatidylinositol anchored proteins from the endoplasmic reticulum to the cell surface. *J Lipid Res*. 2016;57:352-60.

Nagata T, Okada K, Takebe I et al. Delivery of tobacco mosaic virus RNA into plant protoplasts mediated by reverse-phase evaporation vesicles (liposomes). Mol Gen Genet 1981;184:161-65.

Norman P, Wingate V, Fitter M et al. Monoclonal-antibodies to plant plasma-membrane antigens *Planta* 1986;167:452-59.

Oda Y, Asatsuma S, Nakasone H et al. Sucrose starvation induces the degradation of proteins in trans-Golgi network and secretory vesicle cluster in tobacco BY-2 cells. *Biosci Biotechnol Biochem* 2020;84:1652-66.

Ogawa-Ohnishi M, Matsubayashi Y. Identification of three potent hydroxyproline O-galactosyltransferases in Arabidopsis. *Plant J* 2015;81:736-46.

Oka T, Saito F, Shimma Y et al. Characterization of endoplasmic reticulum-localized UDP-D-galactose: hydroxyproline O-galactosyltransferase using synthetic peptide substrates in *Arabidopsis*. *Plant Physiol* 2010;152:332-40.

Paris N, Rogers SW, Jiang L et al. Molecular cloning and further characterization of a probable plant vacuolar sorting receptor. *Plant Physiol* 1997;115:29-39.

Parsons HT, Stevens TJ, McFarlane HE et al. Separating Golgi proteins from *cis* to *trans* reveals underlying properties of cisternal localization. *Plant Cell* 2019;31:2010-34.

Pereira AM, Pereira LG, Coimbra S. Arabinogalactan proteins: rising attention from plant biologists. *Plant Reprod* 2015;28:1-15.

Poulsen CP, Dilokpimol A, Geshi N. Arabinogalactan biosynthesis: Implication of AtGALT29A enzyme activity regulated by phosphorylation and co-localized enzymes for nucleotide sugar metabolism in the compartments outside of the Golgi apparatus. *Plant Signal Behav* 2015;10:e984524.

Poulsen CP, Dilokpimol A, Mouille G et al. Arabinogalactan glycosyltransferases target to a unique subcellular compartment that may function in unconventional secretion in plants. *Traffic* 2014;15:1219-34.

Putoczki TL, Pettolino F, Griffin MD et al. Characterization of the structure, expression and function of *Pinus radiata* D. Don arabinogalactan-proteins. *Planta* 2007;226:1131-42.

Sonobe S. Cytochalasin B cytokinetic cleavage in miniprotoplast isolated from cultured tobacco cells. *Protoplasma* 1990;155:239-42.

Shimizu M, Igasaki T, Yamada M et al. Experimental determination of proline hydroxylation and hydroxyproline arabinogalactosylation motifs in secretory proteins. *Plant J* 2005;42:877-89.

Showalter AM, Basu D. Extensin and arabinogalactan-protein biosynthesis: glycosyltransferases, research challenges, and biosensors. *Front Plant Sci* 2016;7:814.

Showalter AM, Keppler B, Lichtenberg J et al. A bioinformatics approach to the identification, classification, and analysis of hydroxyproline-rich glycoproteins. *Plant Physiol* 2010;153:485-513.

Silva J, Ferraz R, Dupree P et al. Three decades of advances in arabinogalactan-protein biosynthesis. *Front Plant Sci* 2020;11:610377.

Singh H, Ansari HR, Raghava GP. Improved method for linear B-cell epitope prediction using antigen's primary sequence. *PLoS One* 2013;8:e62216.

Steffan W, Kováčč P, Albersheim P et al. Characterization of a monoclonal antibody that recognizes an arabinosylated (1-]6)-beta-D-galactan epitope in plant complex carbohydrates *Carbohydrate Res* 1995;275:295-307.

Suga S, Imagawa S, Maeshima M. Specificity of the accumulation of mRNAs and proteins of the plasma membrane and tonoplast aquaporins in radish organs. *Planta* 2001;212:294-304.

Tan L, Qiu F, Lamport DT et al. Structure of a hydroxyproline (Hyp)-arabinogalactan polysaccharide from repetitive Ala-Hyp expressed in transgenic *Nicotiana tabacum*. *J Biol Chem.* 2004;279:13156-65.

Tan L, Varnai P, Lamport DT et al. Plant O-hydroxyproline arabinogalactans are composed of repeating trigalactosyl subunits with short bifurcated side chains. *J Biol Chem*. 2010;285:24575-83.

Tasaki M, Asatsuma S, Matsuoka K. Monitoring protein turnover during phosphate starvation-dependent autophagic degradation using a photoconvertible fluorescent protein aggregate in tobacco BY-2 cells. *Front Plant Sci* 2014;5:172.

Temple H, Mortimer JC, Tryfona T et al. Two members of the DUF579 family are responsible for arabinogalactan methylation in Arabidopsis. *Plant Direct* 2019;3:e00117.

Toyooka K, Goto Y, Asatsuma S et al. A mobile secretory vesicle cluster involved in mass transport from the Golgi to the plant cell exterior. *Plant Cell* 2009;21:1212-29.

Tryfona T, Liang HC, Kotake T et al. Structural characterization of Arabidopsis leaf arabinogalactan polysaccharides. *Plant Physiol* 2012;160:653-66.

Uemura T, Nakano RT, Takagi J et al. A Golgi-released subpopulation of the *trans*-Golgi network mediates protein secretion in *Arabidopsis. Plant Physiol* 2019;179:519-32.

Uemura T, Suda Y, Ueda T et al. Dynamic behavior of the *trans*-Golgi network in root tissues of Arabidopsis revealed by super-resolution live imaging. *Plant Cell Physiol* 2014;55:694-703.

Velasquez SM, Ricardi MM, Poulsen CP et al. Complex regulation of prolyl-4-hydroxylases impacts root hair expansion. *Mol Plant* 2015;8:734-46.

Viotti C, Bubeck J, Stierhof YD et al. Endocytic and secretory traffic in Arabidopsis merge in the *trans*-Golgi network/early endosome, an independent and highly dynamic organelle. *Plant Cell* 2010;22:1344-57.

Wilkop T, Pattathil S, Ren G et al. A hybrid approach enabling large-scale glycomic analysis of post-Golgi vesicles reveals a transport route for polysaccharides. *Plant Cell* 2019 ;31:627-44.

Willats WG, Marcus SE, Knox JP. Generation of monoclonal antibody specific to (1-->5)-alpha-L-arabinan. *Carbohydr Res* 1998;308:149-52.

Xu J, Tan L, Lamport DT et al. The O-Hyp glycosylation code in tobacco and Arabidopsis and a proposed role of Hyp-glycans in secretion. *Phytochemistry* 2008;69:1631-40.

Xu Z, Gao Y, Gao C et al. Glycosylphosphatidylinositol anchor lipid remodeling directs proteins to the plasma membrane and governs cell wall mechanics. *Plant Cell* 2022;34:4778–94.

Xue H, Veit C, Abas L et al. Arabidopsis thaliana FLA4 functions as a glycan-stabilized soluble factor via its carboxy-proximal fasciclin 1 domain. *Plant J* 2017;91:613-30.

Yamauchi N, Gosho T, Asatuma S et al. Polarized localization and borate-dependent degradation of the *Arabidopsis* borate transporter BOR1 in tobacco BY-2 cells. *F1000Res* 2013;2:185.

Yates EA, Valdor JF, Haslam SM et al. Characterization of carbohydrate structural features recognized by anti-arabinogalactan-protein monoclonal antibodies. *Glycobiology* 1996;6:131-9.

Yeats TH, Bacic A, Johnson KL. Plant glycosylphosphatidylinositol anchored proteins at the plasma membrane-cell wall nexus. *J Integr Plant Biol* 2018;60:649-69.

Yuasa K, Toyooka K, Fukuda H et al. Membrane-anchored prolyl hydroxylase with an export signal from the endoplasmic reticulum. *Plant J* 2005;41:81-94.

Zhou K. The regulation of the cell wall by glycosylphosphatidylinositol-anchored proteins in *Arabidopsis*. *Front Cell Dev Biol* 2022;10:904714.

Figures and legends

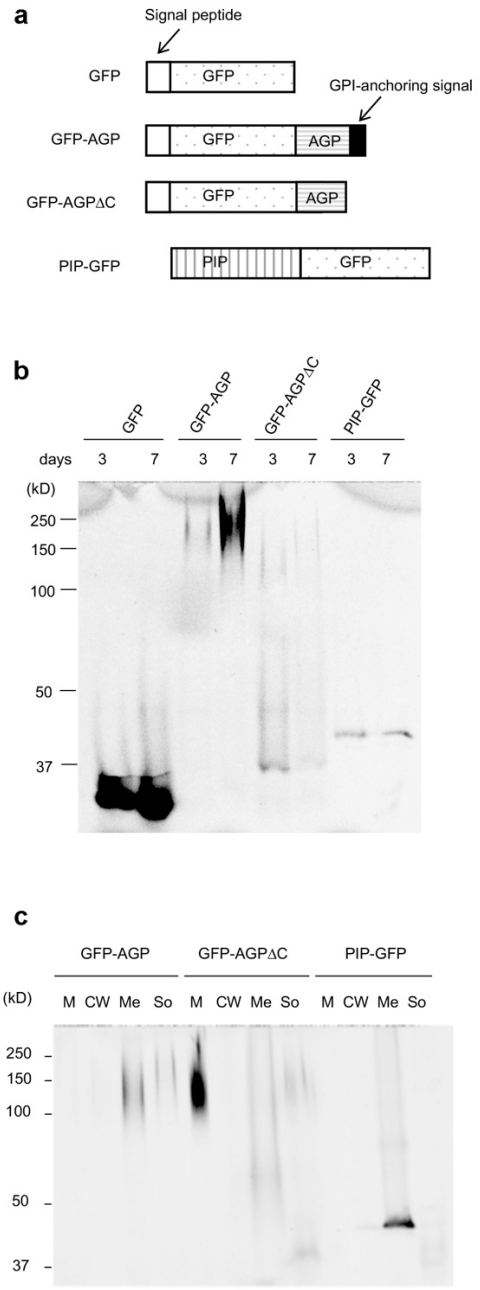

Fig. 1. Expression of the GFP-AGP fusion protein and its mutant without a GPI-anchoring signal in tobacco BY-2 cells.

(a) Schematic representation of the GFP fusion constructs. (b) Accumulation of GFP fusion proteins in the culture of transformed tobacco cells. Total cell lysates were prepared from cells from 3-day and 7-day cultures, then separated by SDS-PAGE, and the GFP fluorescence in the gel was recorded. Each lane contained 3.6 μg of protein. (c) Fractionation of 7-day cultures and the distribution of the GFP fusion proteins. Each lane contained proteins corresponding to 40 μL of cell culture. M: medium fraction, CW: cell wall fraction, Me: membrane fraction from total cell lysate, So: soluble fraction from total cell lysate.

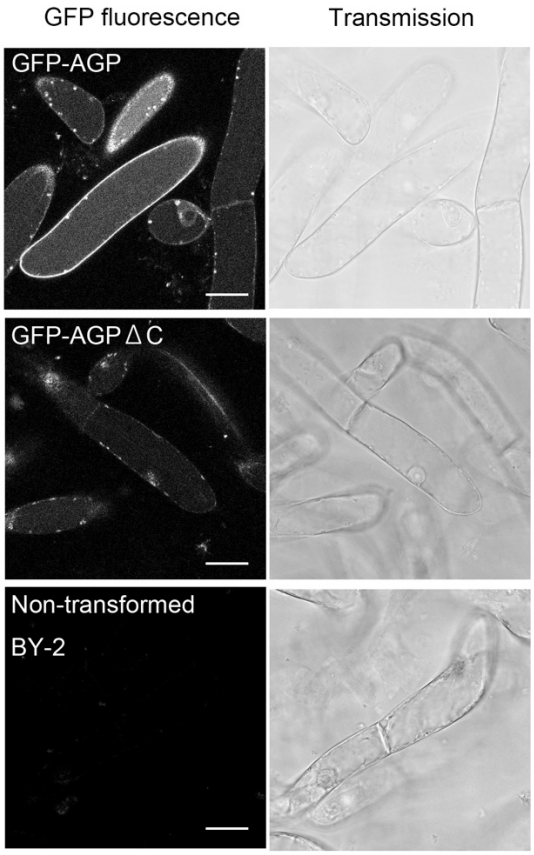

Fig. 2. Confocal localization study of GFP-AGP and GFP-AGPΔC in transformed tobacco BY-2 cells

Confocal image of 7-day-old transformed tobacco cells expressing GFP-AGP, GFP-AGPΔC, or non-transformed cells. *Left:* Confocal fluorescence image and (*right*) the corresponding DIC image. Bars: 30 μm.

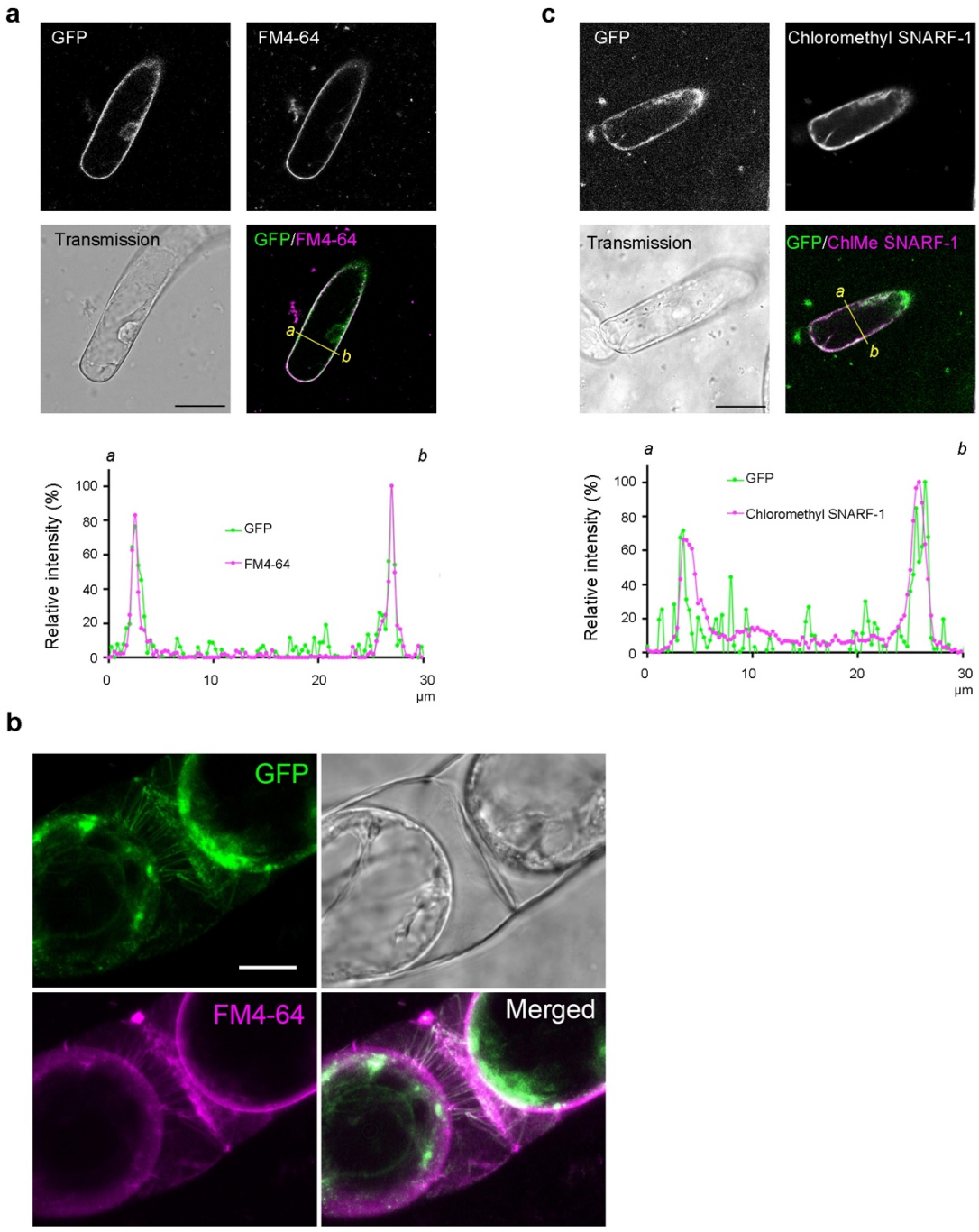

Fig. 3. Comparison of the localization of GFP-AGP and plasma membrane or cytosol markers

(a) Comparison of GFP-AGP and plasma membrane marked with FM4-64. Cells expressing GFP-AGP were incubated for 5 min with FM 4-64, then the fluorescence of both GFP and FM 4-64 was recorded using CFLM. The intensities of the fluorescence signals along the *yellow line* in the merged image were quantified. Normalized (maximum as 100%) intensities are shown in the graph. (b) Confocal image of cells expressing

GFP-AGP after staining with FM4-64 and plasmolysis. Composite images from 23 Z-stack images encompassing 7.96 μm are shown for GFP-AGP and FM 4-64 signals. (c) Comparison of GFP-AGP and cytoplasm marked with 5- (and 6-) chloromethyl SNARF-1. Cells expressing GFP-AGP were incubated with 5- (and 6-) chloromethyl SNARF-1 acetate (SNARF) for 5 min; confocal images were collected, and the intensities of the signals were quantified as in panel a. Bars: 30 μm in a and c, and 10 μm in b.

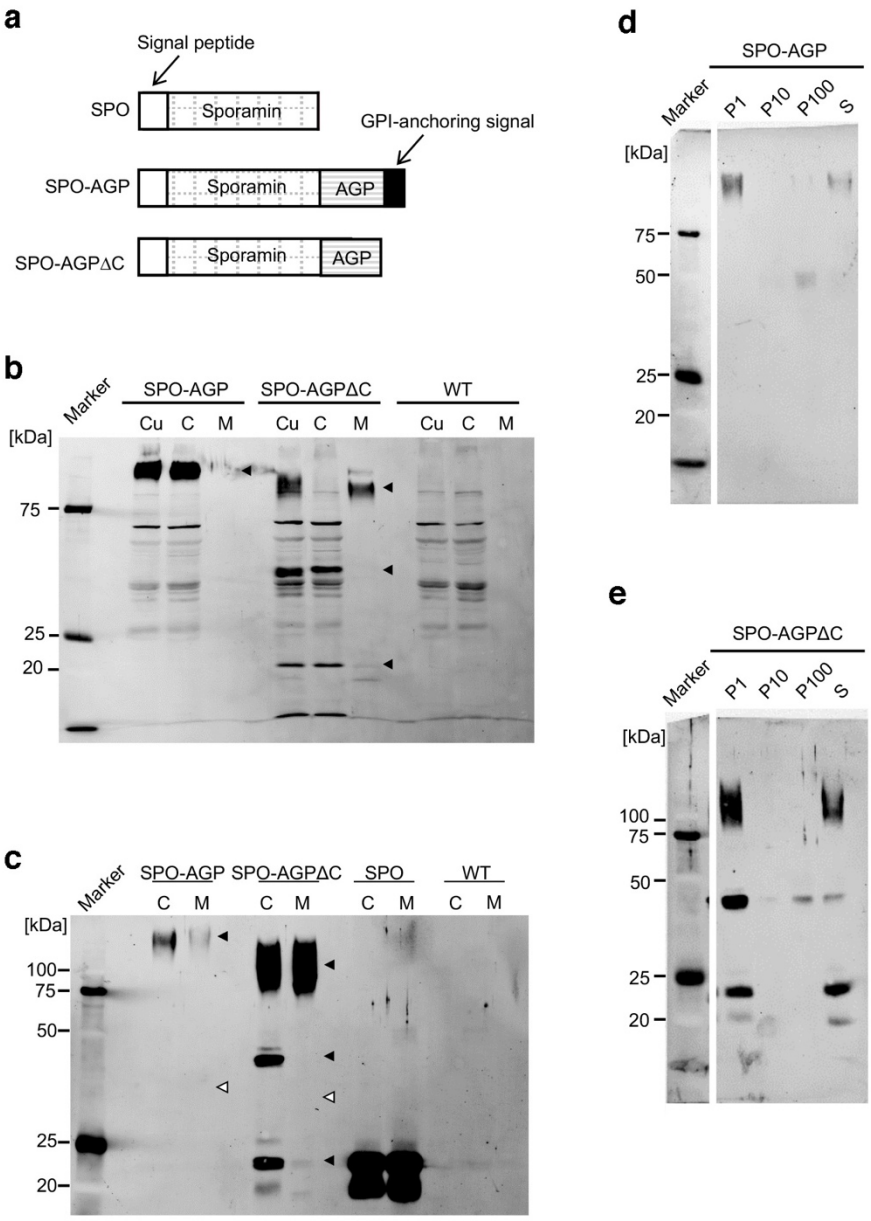

Fig. 4. The expression, secretion, and subcellular localization of the SPO-AGP fusion protein and its mutant lacking a GPI-anchoring signal in tobacco BY-2 cells

(a) Schematic representation of the SPO fusion constructs. (b) Expression and secretion of SPO-AGP and SPO-AGPΔC. Seven-day-old cultures (Cu) of transformed BY-2 cells expressing SPO-AGP and SPO-AGPΔC and non-transformed BY-2 cells (WT) were separated into cells (C) and medium (M). The proteins in these

fractions, corresponding to 10 μL of cell culture, were separated by SDS-PAGE, and SPO-related polypeptides were detected by using an anti-SDS-denatured SPO antibody. *Closed arrowheads:* transgene-dependent polypeptides. (c) Detection of SPO-related polypeptides after immunoprecipitation. SPO-related polypeptides were recovered by immunoprecipitation using immobilized anti-native SPO, and the recovered proteins were analyzed by immunoblotting as described in the Materials and Methods section. Each lane contained SPO-related polypeptides from 0.5 mL of 7-day-old culture. *Closed arrowheads:* the migration position of transgene-dependent polypeptides detected in panel b. *Open arrowheads:* the calculated migration position of non-glycosylated polypeptides. (d) Subcellular fractionation study of SPO-AGP-expressing cells. Fractionation of cells was carried out by differential centrifugation as described in the Materials and Methods, and SPO-related polypeptides in the fractions were recovered by immunoprecipitation, separated by SDS-PAGE, and detected by immunoblotting. P1: the 1,000*g* precipitate containing cell walls and unbroken cells, P10: the 10,000*g* precipitate containing most of the mitochondria, P100: the 100,000*g* precipitate containing microsomes, S: the 100,000*g* supernatant containing soluble proteins in the cytoplasm, vacuoles and periplasmic space. (e) Subcellular fractionation study of SPO-AGPΔC-expressing cells. The subcellular fractionation and detection of SPO-related polypeptides were carried out as in panel d.

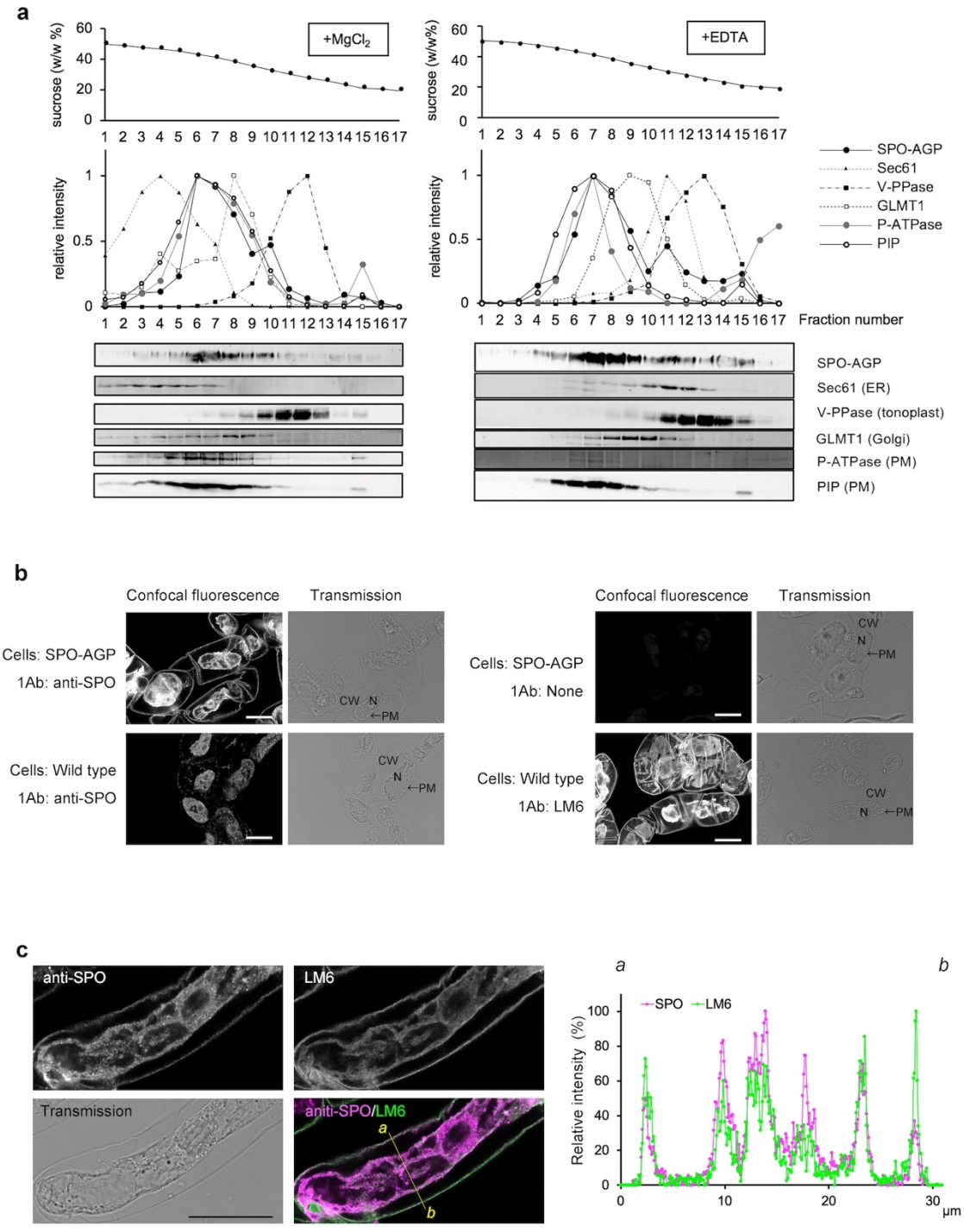

Fig. 5. Intracellular distribution of SPO-AGP

(a) Microsomes were prepared from SPO-AGP-expressing cells in the presence of Mg^{2+} or EDTA and subjected to isopycnic sucrose density gradient ultracentrifugation. The resulting gradients were fractionated from the bottom into 17 fractions. The concentration of sucrose in the gradient is shown at the top. The

distribution of marker proteins was analyzed by immunoblotting with specific antibodies: P-ATPase and PIP for PM, Sec61 for the ER, GLMT1 for the Golgi apparatus, and V-PPase for the vacuolar membrane. The distribution of SPO-AGP, which migrated close to the top of the gel, was analyzed by immunoblotting using an antibody against SPO. *Middle panels:* the relative distribution of SPO-AGP and marker proteins after quantification of the signals on blots. *Bottom panels:* the immunoblot results. (b) Immunostaining of SPO-AGP-expressing or non-transformed cells with anti-native SPO antibody or anti-AGP glycan LM6. (c) Colocalization of SPO-AGP and anti-AGP glycan epitope. SPO-AGP-expressing cells were stained with both anti-native SPO antibody and anti-AGP glycan LM6 with appropriate secondary antibodies. *Left:* Confocal images of both stained and corresponding transmission images. Intensities of the fluorescence signals along the *yellow line* in the merged images were quantified. Normalized (maximum as 100%) intensities are shown in the graph.

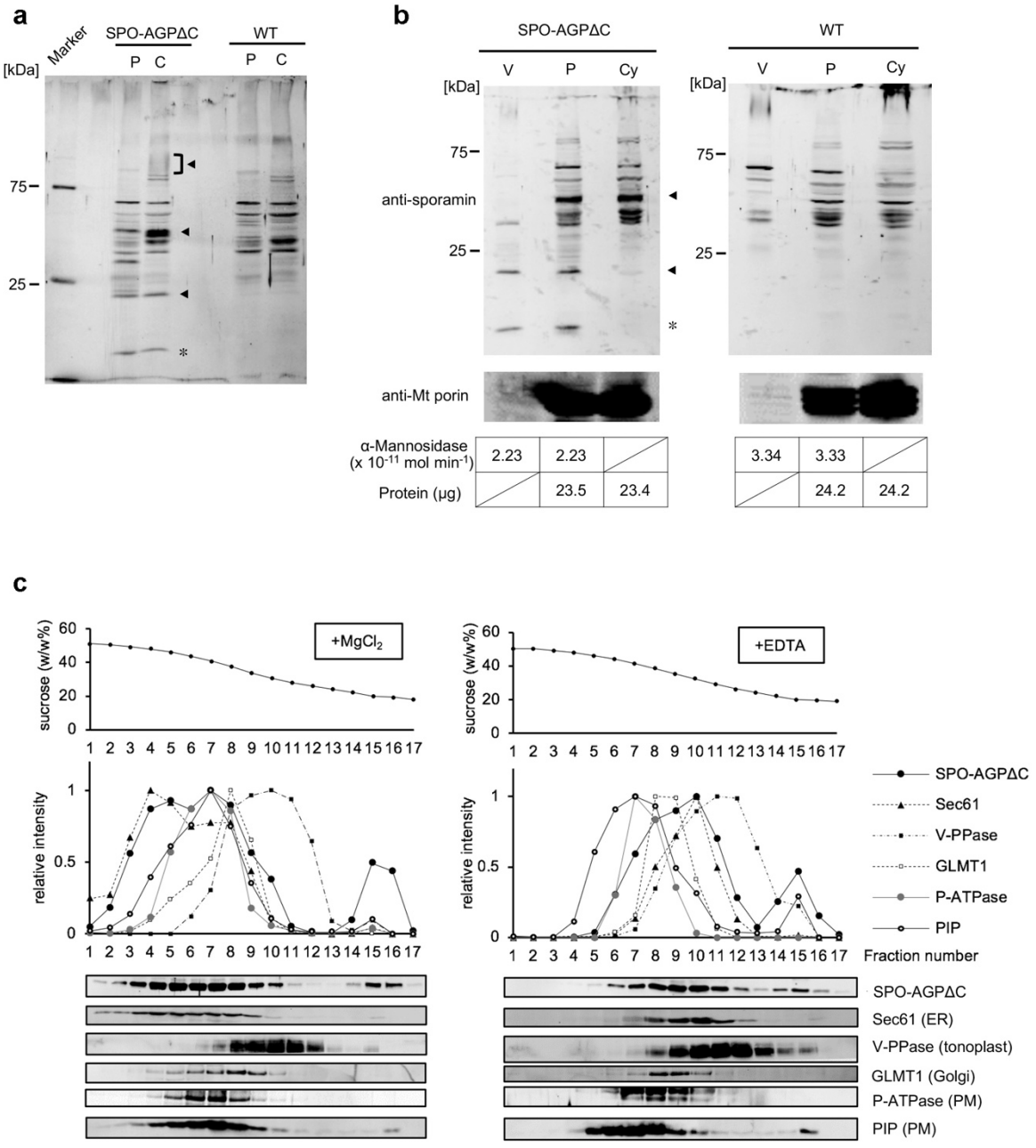

Fig. 6. Distribution of different forms of SPO-AGPΔC in the cell

(a) Distribution of different forms in cells and protoplasts. Protoplasts were prepared from SPO-AGPΔC-expressing cells by digesting the cell walls as described in the Materials and Methods. Proteins in cells and protoplasts were separated by SDS-PAGE, and SPO-related polypeptides were detected by immunoblotting. As a control, protoplasts were prepared from non-transformed cells (WT), and cross-reactive polypeptides against

anti-SPO were analyzed by immunoblotting. Each lane contained 25 μg of protein. *Closed arrowheads:* the migration position of the transgene-dependent polypeptides. *Asterisks:* a possible degradation product of SPO that was occasionally observed on immunoblots. C, cells; P, protoplasts. (b) The small form of SPO-AGPΔC was localized in the vacuoles. To assess the localization of the intermediate and small SPO-AGPΔC proteins, protoplasts were separated into vacuoplasts and cytoplasts, and the distribution of SPO-AGPΔC proteins was analyzed by immunoblotting. A nearly equal amount of the activity of α-mannosidase, which is a vacuolar marker enzyme, was loaded in the vacuoplast and protoplast lanes, and nearly equal amounts of proteins were loaded into the protoplast and cytoplast lanes. As a fractionation control, mitochondrial porin was also detected by immunoblotting. Cy cytoplasts; P, protoplasts, V, vacuoplasts. (c) The distribution of the intermediate form of SPO-AGPΔC within endomembrane organelles. Microsomes were prepared from SPO-AGPΔC-expressing cells in the presence of Mg^{2+} (*left*) or EDTA (*right*), subjected to isopycnic sucrose density gradient ultracentrifugation, fractionated, and analyzed for the distribution of intermediate SPO-AGPΔC and marker proteins as described in the Fig. 5a legend.

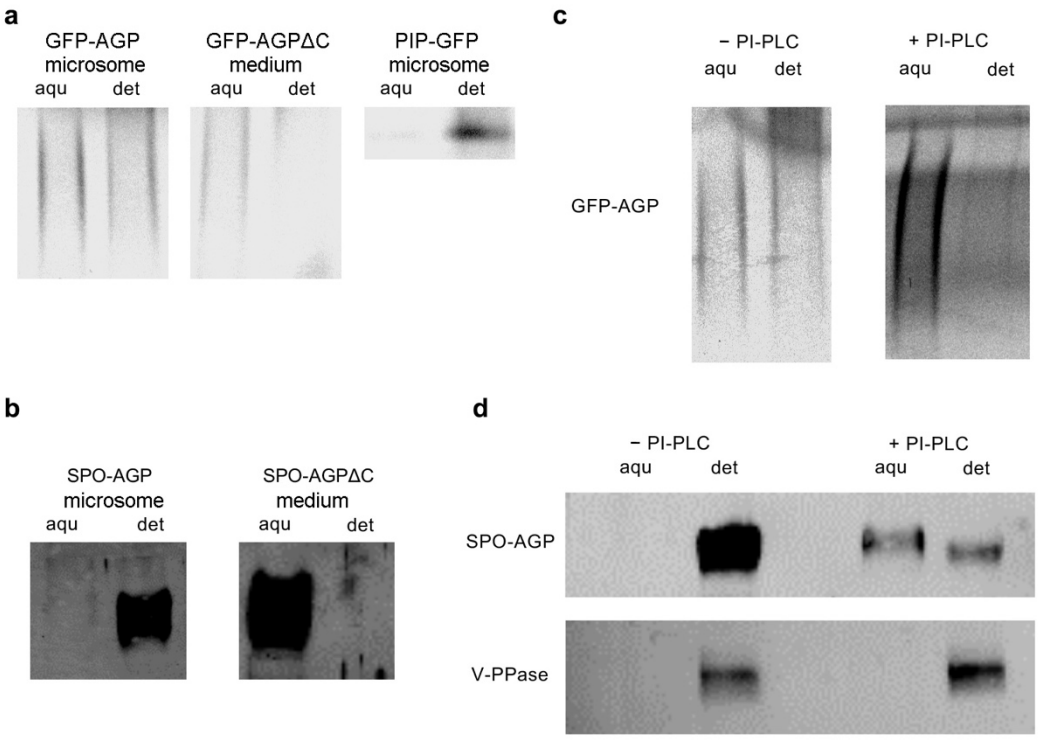

Fig. 7. Both GFP-AGP and SPO-AGP are GPI-anchored proteins

(a) Triton X-114 two-phase partition assay of GFP-AGP, GFP-AGPΔC and PIP-GFP. Microsomes from GFP-AGP- or PIP-GFP-expressing cells and the culture medium of GFP-AGPΔC-expressing cells was subjected to the two-phase separation assay as described in the Materials and Methods. Proteins in these two phases were separated by SDS-PAGE, and the fluorescence of GFP in the gel was recorded. Each lane contained proteins corresponding to an equal amount of microsomes or medium. aqu: aqueous phase, det: detergent phase. (b) Triton X-114 two-phase partition assay of SPO-AGP and SPO-AGPΔC. Two-phase partition was carried out as described in the legend for panel A. Proteins were separated by SDS-PAGE and detected by immunoblotting using anti-SPO antibody. (c) PI-PLC digestion of GFP-AGP. The two-phase partition assay was carried out in the absence and presence of PI-PLC. (d) Two-phase partition assay of SPO-AGP. Microsomal proteins from SPO-AGP-expressing cells were subjected to the second-round two-phase partition assay in the absence or presence of PI-PLC. Both SPO-AGP and V-PPase, which is an integral membrane protein, were detected by

immunoblotting. Each lane in these figures contained proteins corresponding to an equal amount of microsomes or medium.

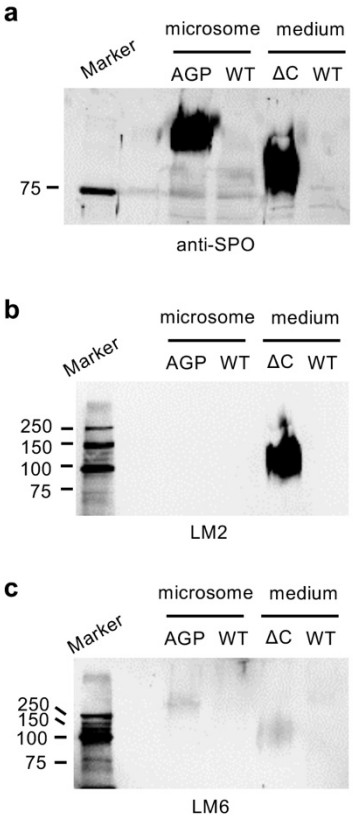

Fig. 8. The large form of SPO-AGPΔC was specifically recognized by LM2 monoclonal antibody

(a) The detection by anti-SPO antibody showed that nearly equal amounts of SPO-fusion proteins were loaded. (b) Detection by the monoclonal antibody LM2, which recognizes a glycan epitope with b-linked glucuronic acid. (c) Detection by the monoclonal antibody LM6, which recognizes a glycan epitope consisting of (1-5)-α-L-arabinosyl residues. AGP: microsomes from SPO-AGP-expressing cells, ΔC: culture medium from SPO-AGPΔC expressing culture, WT: corresponding microsomes and medium from non-transformed BY-2 cells with an equal amount of protein with either microsomes from SPO-AGP or culture medium from SPO-AGPΔC.

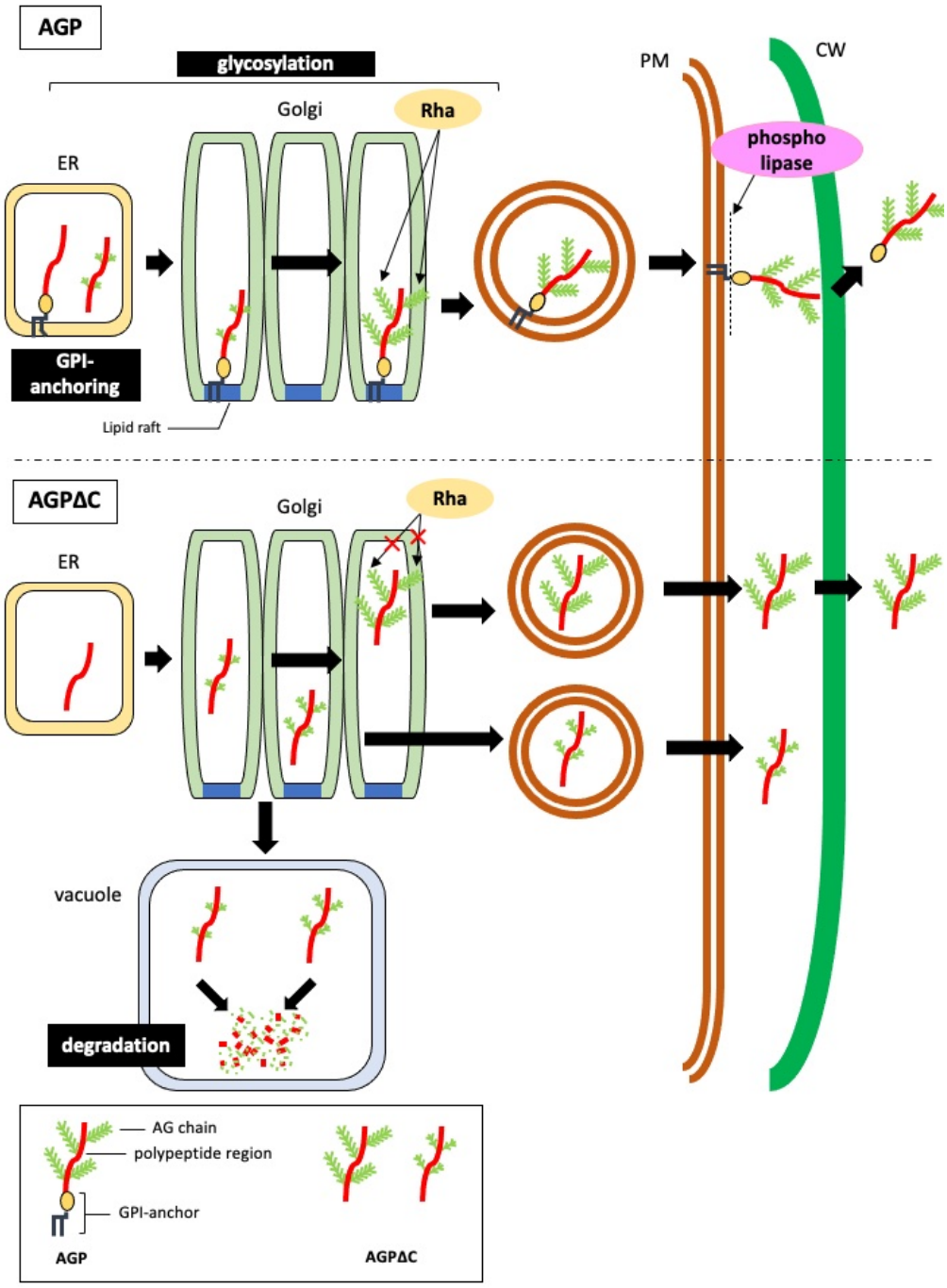

Synthesis, transport, and modification of arabinogalactan protein (upper), and its mutant without GPI-anchoring signal (lower) in tobacco BY-2 cells.

Graphical Abstract

Synthesis, transport, and modification of arabinogalactan protein (upper), and its mutant without GPI-anchoring signal (lower) in tobacco BY-2 cells.

Supplemental figures

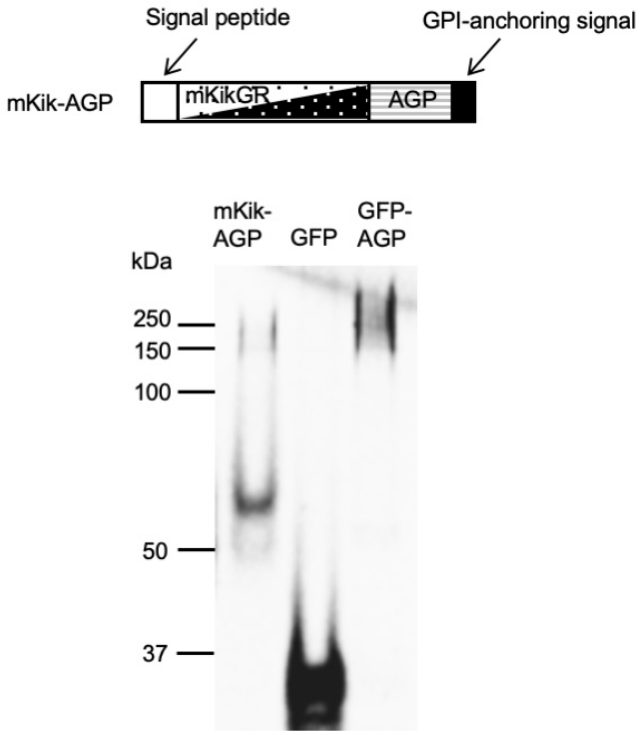

Nagasato *et al.*, Supplemental figure S1

Suppl. Fig. S1. Expression of the monomeric kikume green-red (mKikGR)-AGP fusion protein in tobacco BY-2 cells. Proteins were extracted from transformed tobacco BY-2 cells expressing mKikGR-AGP, GFP, or GFP-AGP and separated by SDS-PAGE. The green fluorescence in the gel emitted from these proteins was then recorded using a Typhoon 9600 image analyser.

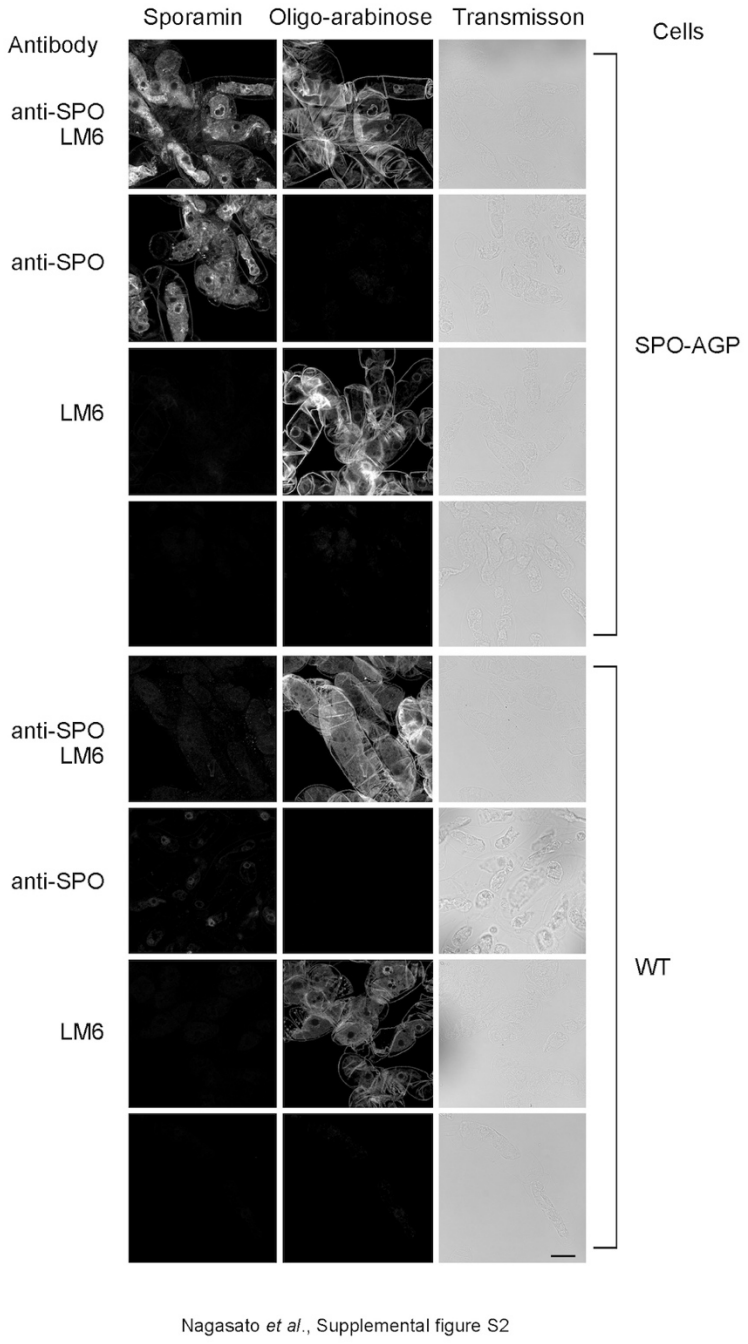

Suppl. Fig. S2. Immunostaining of SPO-AGP-expressing cells (SPO-AGP) and non-transformed tobacco BY-2 cells (WT) with anti-sporamin and/or LM6 antibodies to detect sporamin-related epitopes and oligo-arabinose epitope, respectively. Confocal fluorescence images were collected using a Leica SP8 microscope with the same condition for all samples, and the adjustment of the intensities of the images was done with

identical conditions for all images. All images are at the same magnification. Bar at the bottom right image: 30 mm.

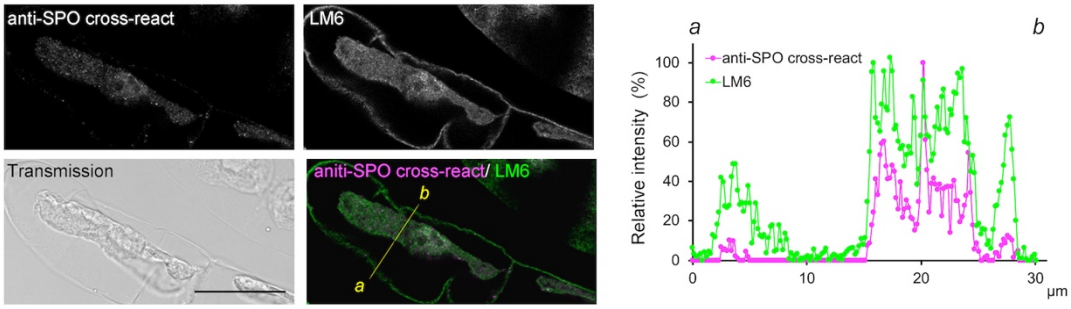

Nagasato *et al.*, Supplemental figure S3

Suppl. Fig. S3. Immunostaining of non-transformed tobacco BY-2 cells (WT) with anti-sporamin and/or LM6 antibodies to detect cross-react signals by anti-sporamin antibody and oligo-arabinose epitope, respectively. Confocal fluorescence images were collected using a Leica SP8 microscope with the same conditions for all samples, and the adjustment of the intensities of the images was done with identical conditions for all images. All images are at the same magnification. Bar at the bottom right image: 30 mm.

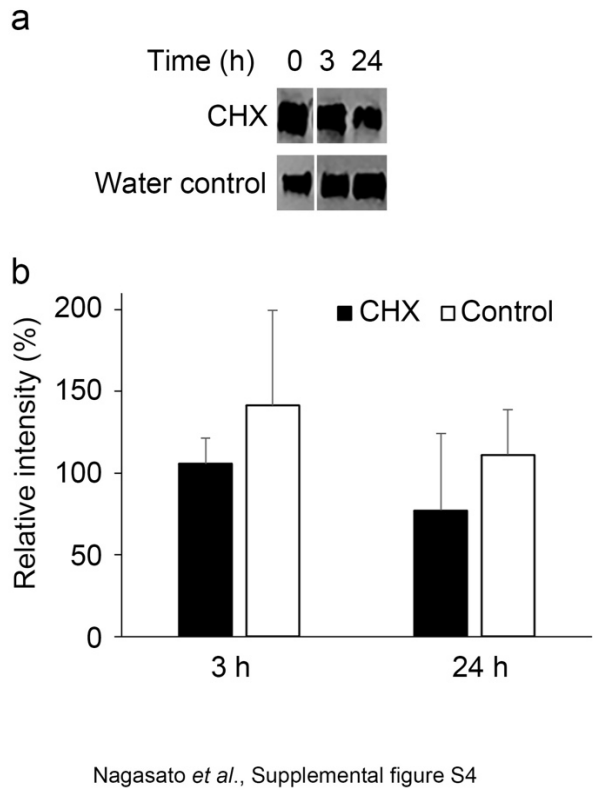

Suppl. Fig. S4. Seven-day culture of SPO-AGP-expressing cells was mixed with a 1/100 volume of cycloheximide (CHX) solution in water at the final concentration of 10 mM or in solvent control (water) and further cultured. At the indicated times, an aliquot of the culture was taken and cellular SPO-AGP was quantified after detection by western blotting. **a:** representative gel image. **b:** the results of the quantification of three independent experiments. Relative intensity to the zero time is shown. No significant difference was observed between CHX and water control by Student's t-test. Bars: SD.

Suppl. Movie S1. Three-dimensional construction of the distribution of GFP-AGP fluorescence in transformed tobacco BY-2 cells. Z-stack images of green fluorescence were collected and reconstituted to the 3D image. The constructed image was rotated.